Journal of Robotics and Control (JRC)
Volume 7, Issue 2, March 2026
ISSN: 2715-5072, DOI: 10.18196/jrc.v7i2.29140

Optimized PI Control for Microgrid Power Management Using a Hybrid Spherical Vector PSO–Differential Evolution Method

Veera Narasimha Murthy Mogilicharla[1*], G. Sambasiva Rao[2]
[1]Research Scholar, Department of Electrical & Electronics Engineering, University college of Engineering and Technology, Acharya Nagarjuna University, Guntur, Andhra Pradesh
[2]Professor, Department of Electrical & Electronics Engineering, R.V.R. & J.C. College of Engineering Chandramoulipuram, Chowdavaram, Guntur, Andhra Pradesh, India
Email: [1] murthyeps@gmail.com
*Corresponding Author

Abstract— **Microgrids play an essential role in supporting reliable and sustainable energy supply, yet their performance is strongly affected by the intermittency of renewable sources such as photovoltaic and wind systems. These variations introduce nonlinear dynamics that challenge conventional control strategies, particularly in maintaining stable active–reactive power flow and DC-link voltage. This study addresses these challenges by optimizing the Proportional–Integral (PI) controller used in a Voltage Source Converter within a hybrid PV–wind–battery microgrid. The research contribution is the development and benchmarking of a hybrid Spherical Vector Particle Swarm Optimization and Differential Evolution (HSPSO-DE) method for PI tuning to improve dynamic response and overall microgrid performance. The microgrid incorporates standard Perturb-and-Observe MPPT for the PV subsystem and an adaptive P&O variant for wind energy to support improved power harvesting, while the battery system ensures load–generation balance during fluctuations. Simulation analysis demonstrates that the HSPSO-DE-tuned PI controller achieves faster convergence, reduced steady-state error, and lower power oscillations when compared with GA, PSO, and GWO-based tuning. Total Harmonic Distortion results confirm improved power quality and enhanced operational stability. The findings establish the proposed hybrid optimization–based PI control as an effective solution for robust microgrid performance under dynamic and uncertain operating conditions.**

Keywords— Microgrid Control; PI Optimization; Hybrid PSO-DE; Renewable Energy Integration; Power Quality

I. INTRODUCTION

The growing demand for reliable, clean, and sustainable electricity has accelerated the adoption of microgrid systems. These localized energy networks, capable of operating either independently or in coordination with the main grid, play a crucial role in integrating distributed energy resources (DERs) such as photovoltaic (PV) arrays, wind turbines, and battery energy storage systems (BESS) [1]. However, the intermittent, nonlinear, and stochastic nature of renewable energy introduces significant challenges related to voltage stability, power quality, and coordinated energy management [2]. Effective control strategies are therefore essential for stable microgrid operation. Among the available techniques, the Proportional–Integral (PI) controller remains widely utilized due to its structural simplicity, ease of implementation, and proven reliability in converter-based systems. PI controllers are commonly employed to regulate DC-link voltage, control active and reactive power flow in Voltage Source Converters (VSCs), and maintain overall system stability [3]. Despite these advantages, conventionally tuned PI controllers often struggle under highly dynamic conditions typical of renewable-rich microgrids. Their fixed gain values cannot adequately adapt to rapid fluctuations in generation and load, resulting in increased steady-state error, slower settling times, and degraded transient performance [4].

To address these limitations, numerous optimization techniques have been introduced to enhance PI controller performance. Classical methods like Genetic Algorithm (GA), Particle Swarm Optimization (PSO), and Grey Wolf Optimizer (GWO) have shown promise in tuning PI parameters [5]. The advancement of control strategies for hybrid microgrids has been a growing area of research due to the increasing integration of renewable energy sources. In [6], a conventional PI control scheme was applied in a PV-based microgrid. While the approach ensured basic stability, it lacked adaptability under dynamic load and weather conditions, resulting in performance degradation. Similarly, [7] explored the use of GA for tuning PI controllers in wind-integrated systems, achieving improved stability but suffering from slow convergence and premature stagnation. In [8], PSO was applied for PI tuning in hybrid microgrids. Although it provided faster convergence compared to GA, it frequently fell into local optima in highly nonlinear environments. In [9] presented an improved PSO for power flow control in microgrids, yet its performance was sensitive to the initial population, affecting repeatability. Differential Evolution (DE) was used in [10] to address convergence speed in PI tuning, but its performance deteriorated with an increase in dimensionality. In [11], an Ant Colony Optimization (ACO)-based method improved the efficiency of microgrid control but required high computational resources and exhibited instability in real-time scenarios. A Bat Algorithm for optimizing control parameters in [12] demonstrated improved voltage stability but lacked robustness against sudden disturbances. In [13], a hybrid GA-PSO was introduced to overcome the limitations of individual

algorithms. Though it offered better performance than standalone methods, it required complex parameter tuning and exhibited instability under fluctuating renewable inputs. Fuzzy Logic with PSO is used in [14], which improved decision-making under uncertainty, but the fuzzy rule base design remained heuristic and unscalable. In [15], a Grey Wolf Optimizer (GWO)-based PI controller showed robust performance in microgrid applications, but it suffered from poor exploitation ability near the global optimum.

Whale Optimization Algorithm (WOA) was applied in [16] for MPPT and control parameter tuning, showing smooth convergence but poor response to rapidly changing input scenarios. Reference [17] used a Sine Cosine Algorithm (SCA) for parameter optimization, yet it showed limited exploration capability in higher-dimensional search spaces. An Improved Harmony Search Algorithm was implemented in [18], which provided enhanced diversity but still required manual intervention for convergence control. In [19], Bacterial Foraging Optimization (BFO) improved accuracy in control tuning but was computationally expensive and slow in convergence. Firefly Algorithm (FA) was investigated in [20], improving local search but lacking a mechanism for maintaining solution diversity. In [21], a Jaya algorithm was applied for PI tuning in inverter-based microgrids, offering simplicity but lacking adaptive capability. In [22] evaluated Seagull Optimization Algorithm (SOA) for voltage and frequency control; however, it faced convergence speed limitations under variable loads. In [23], a Cuckoo Search Algorithm (CSA) was tested, which handled nonlinear constraints well but suffered from poor balance between exploration and exploitation. In [24] employed an Enhanced Teaching-Learning-Based Optimization (ETLBO), which showed improved learning ability but required high memory storage and frequent function evaluations. In [25] introduced a hybrid PSO-DE method for power system control, but its effectiveness declined due to insufficient directional guidance in high-dimensional search spaces.

Building on these efforts, [26] proposed a hybrid GWO–DE scheme for microgrid voltage regulation, achieving better convergence but exhibiting high sensitivity to parameter tuning. In [27], a modified WOA–PSO approach was applied for PI tuning, yet it struggled to maintain performance consistency across different loading conditions. A multi-objective GA–PSO framework in [28] considered both power quality and efficiency but introduced significant computational burden, limiting real-time applicability. In [29], a hybrid CSA–DE algorithm improved search capability but required complex control parameter calibration, making practical deployment challenging. An improved SCA–GWO method was reported in [30] for inverter control; however, it showed oscillatory behavior under rapid irradiance variations.

In [31], an adaptive fuzzy–GA approach was used for microgrid power management, enhancing flexibility but depending heavily on expert-designed fuzzy rules. A reinforcement learning-based PI tuning strategy in [32] demonstrated promising adaptability yet required large training datasets and extensive offline computation. In [33], a neural network-based controller was proposed for microgrid stability, but its black-box nature and training complexity limited interpretability and robustness. A model predictive control scheme optimized by DE was introduced in [34], offering strong dynamic performance but at the expense of high online computation. In [35], a hybrid ACO–PSO algorithm improved convergence diversity but remained vulnerable to premature stagnation in highly nonlinear operating regions.

An improved BFO–PSO algorithm in [36] enhanced exploitation capability but suffered from slow initial convergence. In [37], a harmony search–GWO hybrid method was employed for current control in inverters, yet its performance degraded significantly under parameter mismatch. A hybrid TLBO–DE algorithm in [38] provided good steady-state accuracy but displayed overshoot in transient conditions. In [39], a gravitational search algorithm (GSA) was used for PI tuning, yielding acceptable results but struggling with population diversity in later iterations. A memetic PSO variant in [40] attempted to integrate local search, but the additional complexity did not consistently translate to performance gains.

In [41], a shuffled frog leaping algorithm (SFLA) was applied to optimize microgrid controllers, achieving moderate improvement but incurring considerable iteration overhead. A hybrid FA–GWO method in [42] improved voltage stability but required extensive trial-and-error for parameter setting. In [43], a chaotic PSO variant was introduced to enhance exploration, though the chaotic maps complicated reproducibility and tuning. A multi-swarm PSO strategy in [44] improved robustness to local optima but increased communication and coordination complexity among swarms. In [45], a biogeography-based optimization (BBO) approach was implemented for PI tuning, which provided diversity but had slow convergence in refined search stages.

A hybrid PSO–GWO approach was reported in [46] for DC-link voltage regulation, but it showed inconsistent performance under severe disturbances. In [47], an improved Jaya–DE algorithm was proposed, which reduced parameter dependency but still lacked strong exploitation near the optimum. A salp swarm algorithm (SSA)-based controller in [48] displayed good tracking performance under nominal conditions yet deteriorated under large parameter uncertainties. In [49], a grasshopper optimization algorithm (GOA) was applied to microgrid control, but its performance was highly sensitive to population size and control coefficients. A marine predators algorithm-based scheme in [50] offered faster convergence but exhibited instability in low-inertia microgrids.

In [51], a hybrid PSO–GSA method attempted to combine exploration and exploitation but faced difficulties balancing the two across different operating points. An improved DE variant using adaptive scaling factors in [52] enhanced convergence but required careful tuning to avoid divergence. In [53], an equilibrium optimizer was used for PI tuning, showing potential yet lacking extensive validation under diverse scenarios. A hybrid CSA–GWO algorithm in [54] improved constraint handling but suffered from computational complexity. In [55], a metaheuristic based on

moth-flame optimization was tested for microgrid applications, but it showed susceptibility to trap in local optima under nonlinear disturbances.

More recently, [56] employed a tunicate swarm algorithm for inverter control, exhibiting competitive performance but high parameter sensitivity. In [57], a hybrid SSA–FA optimization technique was proposed, yet its gains over simpler methods were marginal considering the added complexity. A physics-inspired optimization approach in [58] provided good theoretical properties but lacked demonstration in realistic, large-scale microgrids. In [59], a hybrid multi-objective evolutionary algorithm addressed power quality and economic dispatch simultaneously, though it was computationally intensive and difficult to implement in real time. Finally, [60] introduced a cooperative co-evolution framework for controller tuning, which improved modularity but required problem-specific decomposition strategies.

Collectively, these studies indicate that while a wide variety of metaheuristic and hybrid algorithms have been applied to microgrid PI tuning, many still suffer from issues such as premature convergence, parameter sensitivity, computational burden, limited scalability, and difficulties in balancing exploration and exploitation. These persistent challenges motivate the need for more geometry-aware, robust, and computationally efficient optimization frameworks such as the proposed HSPSO-DE.

Existing studies on optimization-based PI tuning consistently reveal several unresolved limitations that hinder reliable microgrid operation under dynamic conditions. Many algorithms suffer from premature convergence, insufficient adaptability to nonlinear system variations, slow convergence rates, or extensive parameter tuning requirements. These issues become more pronounced in hybrid microgrids, where the variability of photovoltaic and wind energy sources demands fast, robust, and adaptive control strategies to maintain stable voltage, frequency, and power quality in the presence of uncertainty. Consequently, a more capable optimization framework is required to ensure reliable controller performance in such complex environments. The proposed Hybrid Spherical Vector Particle Swarm Optimization–Differential Evolution (HSPSO-DE) algorithm offers a new direction for enhanced PI controller tuning. A key theoretical advancement lies in the adoption of spherical vector representation within the PSO component. Unlike conventional Cartesian PSO, which restricts particles to axis-aligned movement and often collapses directional diversity, the spherical-vector formulation decomposes particle motion into independent magnitude and angular components. This geometric interpretation enables richer directional exploration, superior boundary handling, and improved capability to escape local optima. Such properties are essential for high-dimensional optimization problems like simultaneous tuning of multiple PI parameters in converter-driven microgrids. By maintaining search diversity while moderating step-size sensitivity, spherical-vector PSO provides a more suitable search landscape for the nonlinear, multi-parameter control problem considered in this study.

Complementing this, Differential Evolution contributes strong exploitation capability through differential mutation and crossover, enabling precise local refinement once promising regions of the search space are identified. The hybrid integration of SVPSO and DE allows the algorithm to capitalize on their complementary strengths: SVPSO drives global exploration and avoids premature convergence, while DE accelerates local convergence and enhances fine-tuning accuracy. This synergy yields a balanced global–local search mechanism that is particularly effective for tuning PI controllers under fluctuating renewable inputs. The HSPSO-DE framework is applied to a PV–Wind–Battery hybrid microgrid, where PI controllers regulate DC-link voltage and active–reactive power flow in the Voltage Source Converter. Standard Perturb and Observe (P&O) MPPT is used for the PV subsystem, whereas an adaptive P&O technique enhances wind energy extraction; however, these MPPT algorithms serve only as supporting components and are not claimed as novel contributions. The battery system dynamically manages charge–discharge behavior to maintain supply–demand balance, ensuring stable operation under varying environmental conditions.

To validate the proposed approach, extensive MATLAB/Simulink simulations are conducted, benchmarking HSPSO-DE against established techniques such as GA, PSO, and GWO. Performance metrics—including transient response characteristics, steady-state error, power fluctuations, and Total Harmonic Distortion (THD)—are analyzed to demonstrate the algorithm's effectiveness. Results consistently show that HSPSO-DE achieves faster convergence, reduced steady-state error, improved dynamic stability, and superior power quality relative to competing methods. These outcomes confirm the algorithm's suitability for real-time control in renewable-rich microgrids.

The main contributions of this work can be summarized as follows:

- Development of a hybrid HSPSO-DE algorithm tailored for high-dimensional PI controller tuning using spherical-vector geometry;
- Integration of P&O and adaptive P&O strategies to support stable renewable energy extraction;
- Comprehensive benchmarking against widely used optimization techniques; and
- Demonstrated improvement in microgrid power quality and stability through THD minimization and enhanced transient response.

The remainder of the paper is organized as follows: Section 2 introduces the hybrid DC microgrid system; Section 3 presents the modeling of individual energy sources; Section 4 details the HSPSO-DE algorithm; Section 5 provides simulation results and discussion; and Section 6 concludes the work with future research directions.

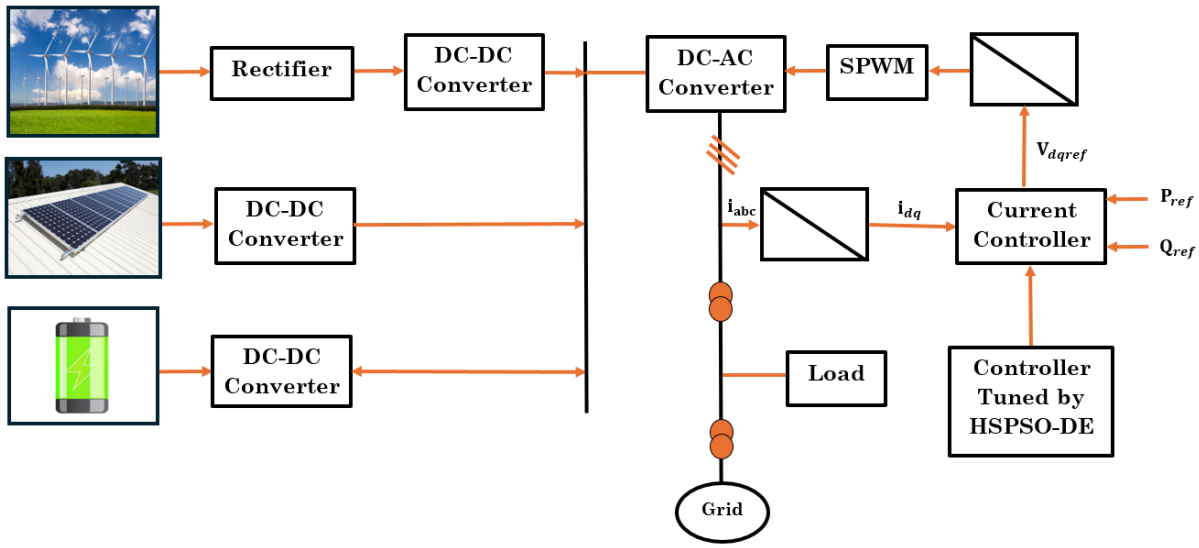

Fig. 1. Hybrid DG system design

II. HYBRID DG SYSTEM (HDGS)

Figure 1 shows the hybrid system, which integrates a PV-Wind-Battery configuration. The microgrid system integrates a WT, PV system, and a battery storage unit, all interconnected to aid efficient energy flow from the DC bus to the utility grid. The PV system is linked to the DC bus via a DC-DC converter that operates under MPPT control to maximize energy extraction from solar irradiance. Similarly, the WT is connected to the DC bus via a rectifier followed by a DC-DC converter, both controlled by an MPPT algorithm to optimize wind energy capture. The battery storage unit is linked to the DC bus through a bidirectional DC-DC converter, enabling it to either store surplus energy or supply power back to the system based on demand. The overall power flow and energy management of this hybrid system—comprising PV, wind, and battery—are determined by the microgrid's operational mode, particularly when operating in grid-connected mode.

In grid-connected mode, the system actively regulates the delivery of active and reactive power to match predefined reference values. This is accomplished through a Voltage Source Inverter (VSI), which interfaces the DC microgrid with the AC utility grid. The VSI is controlled using sinusoidal pulse width modulation (SPWM), ensuring high-quality voltage and current waveforms. To accommodate fluctuating load demands, the control strategy dynamically adjusts power contributions from the grid and distributed energy sources. Ensuring reliable and continuous distribution of active and reactive power requires a well-coordinated power-sharing strategy among the PV system, wind turbine, battery storage, and grid components.

A key factor for system stability is maintaining power balance at two levels: the DC link, where all generation units are interconnected, and the point of common coupling (PCC) with the grid. Maintaining this balance is crucial for the seamless operation and integration of DG units with the main power system. The total DC power supplied by the combined RES must equal the power demanded by the inverter and the load, forming the foundation for real-time energy management within the microgrid. This relationship is expressed as:

$$P_{dc}(t) = P_{WT}(t) + P_{PV}(t) + P_{Bat}(t) \quad (1)$$

P_{WT}: wind generated power, P_{PV}: PV generated power, P_{bat}: terminal power of the battery, P_{dc}: power available at DC bus. The total power generated by the RES is calculated using Equation (1) and integrated into the overall power flow framework of the microgrid. This ensures precise accounting of the contributions from the PV system, wind turbine, and battery storage. Power balance is maintained by comparing the total output from the hybrid sources with the load demand at the AC bus, enabling effective coordination and ensuring stable operation of the microgrid system.

$$P_g(t) = [P_l(t) - P_{hres}(t)] \quad (2)$$

$$P_l(t) = [P_{hres}(t) + P_g(t)] \quad (3)$$

$$Q_g(t) = [Q_l(t) - Q_{hres}(t)] \quad (4)$$

$$Q_l(t) = [Q_{hres}(t) + Q_g(t)] \quad (5)$$

P_g and Q_g: Active and Reactive powers delivered by the grid, P_l and Q_l: Active and Reactive power consumed by the load, P_{hres} and Q_{hres}: generated active and reactive power by the HDGS. Battery power in the storage system varies depending on the duration of its discharge (supplying energy) and charge (storing energy) cycles. Maintaining a stable power balance is challenging due to the unpredictable nature of RES and fluctuating consumer demand. To manage this effectively, a high-performance control strategy is required to regulate power efficiently. Active and reactive power in the system are calculated using the direct (d-axis) and quadrature (q-axis) components of voltage and current.

$$P_l(t) = \frac{3}{2}[v_d * i_d + v_q * i_q] \quad (6)$$

$$Q_l(t) = \frac{3}{2}[v_q * i_d + v_d * i_q] \quad (7)$$

III. MICROGRID CONTROL SYSTEM

A. PV Array

Figure 2 shows a simplified circuit model of a solar panel. In this model, the PV cell is represented as an ideal current source, I_{ph},, combined with series and parallel resistances to capture real-world characteristics. The output current of the solar cell is given by [61]:

$$I = I_{ph} - I_d \tag{8}$$

Here, I represent the output current from the PV panel, I_{ph} is the photon-generated current, and I_d is the diode current. According to semiconductor theory, the current-voltage (I-V) characteristics of a PV cell are described by the Shockley diode equation [62]:

$$I_d = I_s \left[exp \left(\frac{qV_{oc}}{N_s KAT_o} \right) - 1 \right] \tag{9}$$

By substituting Equation (9) into Equation (8), the final expression for the PV output current is derived as [62]:

$$I_d = I_{ph} - I_s \left[exp \left(\frac{qV_{oc}}{N_s KAT_o} \right) - 1 \right] \tag{10}$$

I_s is the diode saturation current, q is the electron charge, V_{oc} is the open-circuit voltage, N_s represents the number of series-connected cells in the module, K is Boltzmann's constant, and T_o is the nominal cell temperature in Kelvin.

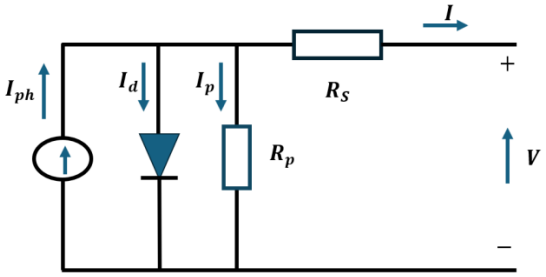

Fig. 2. Equivalent circuit of real model for PV panel

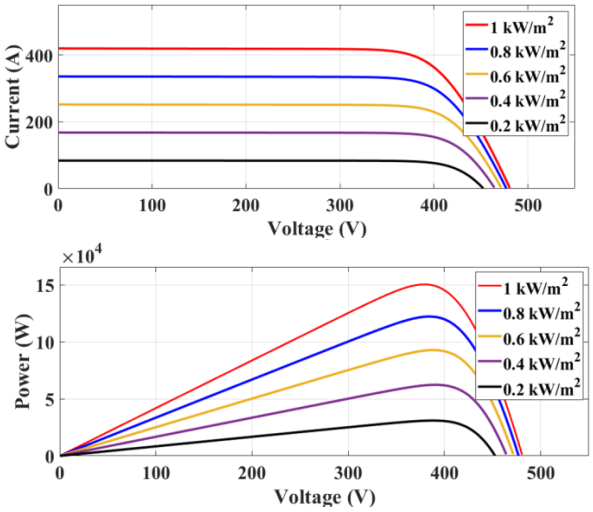

Fig. 3. I-V and P-V characteristics of PV Array

PV power output is highly sensitive to variations in weather conditions such as irradiance and temperature. To maintain a stable output voltage and maximize power generation, a DC-DC converter is employed. Figure 3 highlights the importance of aligning the PV voltage with the maximum power point voltage (V_{mpp}) to extract the highest possible power from the PV arrays. To accomplish this, the system employs the Perturb and Observe (P&O) MPPT algorithm. This algorithm continuously adjusts the duty cycle of the DC-DC converter to maintain the PV voltage at V_{mpp}, ensuring optimal power output. Figure 4 shows the configuration of the DC-DC converter used in the PV system.

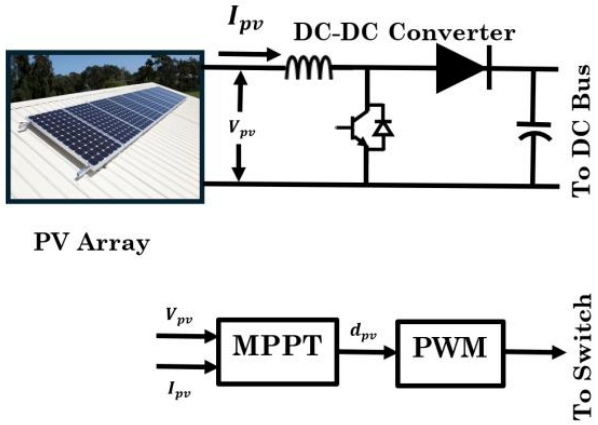

Fig. 4. PV system with boost converter

B. PMSG and Wind Turbine

The output power from a WT, P_ω, is taken by the following equation [63]:

$$P_\omega = \frac{1}{2} \rho A C_p(\lambda, \beta) V_\omega^3 \tag{11}$$

Here, ρ is the air density, A is the swept area of the turbine blades, V_ω is the wind speed, λ is the tip speed ratio, and β is the blade pitch angle. The tip speed ratio λ is estimated as:

$$\lambda = \frac{r_\omega}{V_\omega} \tag{12}$$

where r is the blade radius and ω is the angular speed of the rotor.

The mechanical power generated by the WT can be optimized by adjusting the tip speed ratio (λ) and the pitch angle (β). For a given pitch angle, there is a specific tip speed ratio that maximizes the power coefficient C_p, known as $C_{p,opt}$. This optimal condition is achieved when $\beta = 0$ and the turbine operates at the optimal tip speed ratio λ_{opt}.

The electrical power generated by the wind turbine is harnessed using a Permanent Magnet Synchronous Generator (PMSG) connected to a diode bridge rectifier. The rectified output is then regulated using a DC-DC boost converter, which is controlled by a MPPT algorithm. To enhance system performance and tracking speed, an adaptive version of the P&O MPPT algorithm is employed [64]. This adaptive method dynamically adjusts the step size based on variations in rotor speed and inertia.

The optimal rotor speed ω_{optm} is assessed by:

$$\omega_{opt_m} = \frac{\lambda_{opt} V_w}{R} \tag{13}$$

Instead, it can be stated relative to a base wind speed v_{base} and corresponding base rotor speed ω_{basem}:

$$\omega_{opt_m_p} = \omega_{base_m} \frac{v_w}{v_{base}} \quad (14)$$

If the actual rotor speed ω_m deviates from the optimal value, the control system adjusts it by an adaptive ratio R_{adp}, determined as:

$$R_{adp} = K_{per} \left(\frac{\omega_{opt_m_p} - \omega_m}{\omega_{opt_m_p}} \right) \quad (15)$$

Here, K_{per} is a perturbation constant used to fine-tune the rotor speed.

Once the desired rotor speed is regulated, a PI controller generates the reference torque τ_{opt_m}:

$$\tau_{opt_m} = K_{p1} \left(\omega_{opt_m}(t) - \omega_m(t) \right) + K_{i1} \int \left(\omega_{opt_m}(t) - \omega_m(t) \right) dt \quad (16)$$

This reference torque is used to compute the reference input current I_{wref} for the DC-DC converter:

$$I_{wref} = \tau_{opt_m} \frac{\omega_m}{V_{dcw}} \quad (17)$$

The converter's duty cycle d_w is then assessed by another PI controller:

$$d_w = K_{p2} \left(I_{Wref}(t) - I_W(t) \right) + K_{i2} \int \left(I_{Wref}(t) - I_W(t) \right) dt \quad (18)$$

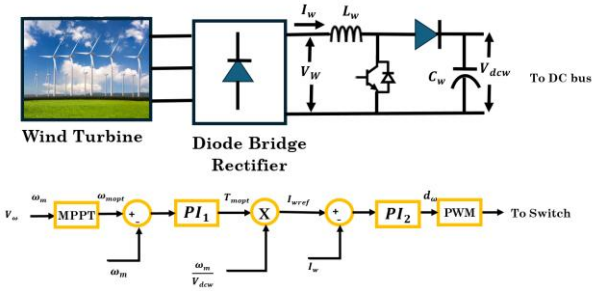

Fig. 5. Wind generation system with boost converter

The duty cycle is used to control the IGBT switch in the DC-DC converter. Figure 5 presents the complete wind energy system, comprising the PMSG, diode rectifier, MPPT-controlled DC-DC converter, and associated control loops.

C. Battery energy storage system (BESS)

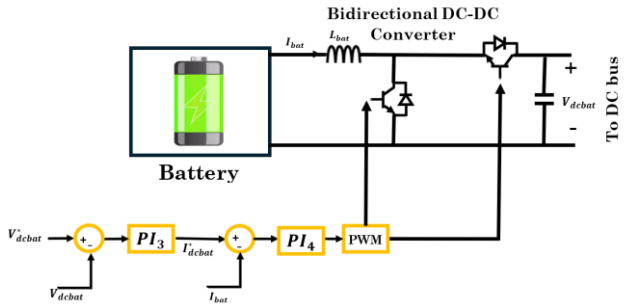

Fig. 6. BESS with DC-DC converter

The bidirectional converter of the BESS regulates the voltage across the DC bus [65]. The DC bus voltage is used as feedback and compared with a reference DC voltage to generate a reference DC current. As showed in Figure 6, the PI₃ controller generates the battery reference current, I_{batref} as follows:

$$I_{batref} = K_{p3} \left(V_{batref}(t) - V_{dcbat}(t) \right) + K_{i3} \int \left(V_{batref}(t) - V_{dcbat}(t) \right) dt \quad (19)$$

K_{p3} and K_{i3} are gains of PI regulator, V_{batref} reference value and V_{dcbat} real value of battery voltage,

PI_4 controller generates duty cycle given as

$$d_{bat} = K_{p4} \left(I_{batref}(t) - I_{bat}(t) \right) + K_{i4} \int \left(I_{batref}(t) - I_{bat}(t) \right) dt \quad (20)$$

K_{p4} and K_{i4} are gains of PI regulator, I_{batref} reference value and I_{bat} real value of battery current,

D. Inverter controlling

Figure 7 presents the controlling approach of the inverter.

To ensure accurate control of active and reactive power within the system, 2 PI controllers are applied to the reference current signals. These controllers are defined by the following equations [66]:

- **Reference direct-axis current**:

$$i_{dref} = K_{p5} \left(P_{ref}(t) - P(t) \right) + K_{i5} \int \left(P_{ref}(t) - P(t) \right) dt \quad (21)$$

- **Reference quadrature-axis current**:

$$i_{qref} = K_{p6} \left(Q_{ref}(t) - Q(t) \right) + K_{i6} \int \left(Q_{ref}(t) - Q(t) \right) dt \quad (22)$$

Here, P_{ref} and Q_{ref} are the reference active and reactive power values, while P and Q are the actual values. K_{p5}, K_{i5}, K_{p6} *and* K_{i6} are the PI controller gains.

The outputs of these controllers generate the required reference currents for the inverter, enabling precise power tracking and minimizing current ripple. To further improve system performance, two additional PI controllers are employed to correct any discrepancies between the reference and actual inverter currents. These control loops incorporate feedback from the inverter current and feedforward from the grid voltage, enhancing both steady-state accuracy and dynamic response.

The voltage reference vectors are stated as:

- **Direct-axis voltage reference**:

$$v_{dref} = K_{p7} \left(i_{dref}(t) - i_d(t) \right) + K_{i7} \int \left(i_{dref}(t) - i_d(t) \right) dt \quad (23)$$

- **Quadrature-axis voltage reference**:

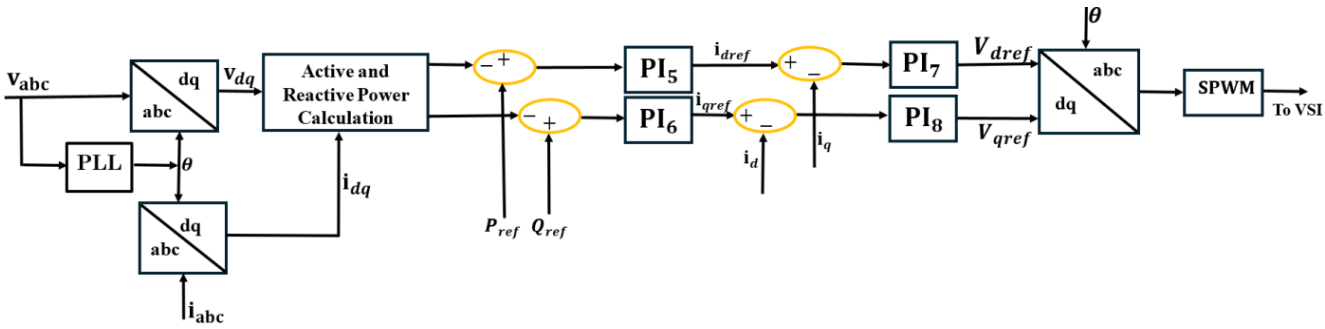

Fig. 7. Controlling approach of the Inverter

$$v_{qref} = K_{p8}\left(i_{qref}(t) - i_q(t)\right) + K_{i8}\int\left(i_{qref}(t) - i_q(t)\right)dt \quad (24)$$

Here, i_d and i_q represent the actual direct and quadrature axis currents, respectively, while K_{p7}, K_{i7}, K_{p8} *and* K_{i8} are the proportional and integral gains of the respective PI controllers. The resulting reference voltages are fed into the PWM system, which generates the inverter's switching signals. This process minimizes harmonic distortion and ensures stable, efficient system operation.

In grid-connected mode, the hybrid distributed generation system (HDGS) adjusts the inverter current's magnitude and phase to deliver the required active and reactive power to the grid. This is accomplished using a control strategy centred on frequency and voltage regulation. HDGS performance is assessed by analyzing the outputs of the PV array, wind turbine, and battery storage. Central to stable and efficient operation is the precise tuning of PI controllers, which regulate critical process variables throughout the system.

To automate and enhance PI controller tuning, heuristic optimization algorithms are utilized. These algorithms search for optimal combinations of controller gains by minimizing performance criteria such as the Integral of Time-weighted Absolute Error (ITAE) [67], overshoot, and settling time. The success of this approach relies on clearly defining the objective function based on control system goals and carefully selecting key optimization parameters such as population size and mutation rate. Conducting multiple optimizations runs helps ensure the robustness and reliability of the resulting controller settings.

Design optimization seeks to identify the optimal configuration by minimizing an objective function, adjusting design variables, and satisfying defined constraints. When multiple objectives are present, the task becomes a multi-objective optimization problem, which is more complex than single-objective cases due to the need to balance potentially conflicting goals. To address this complexity, multi-objective optimization methods—such as the weighted-sum technique—convert several objectives into a single composite function. Each individual objective is assigned a weight and combined according to:

$$F_{objective} = a_1F_1 + a_2F_2 + \cdots + a_nF_n \quad (25)$$

Here $a_1, a_2 \ldots, a_n$, are the weights assigned to each objective. When these weights lie between 0 and 1 and sum to one, they create a convex combination, enabling exploration of various optimal points along the Pareto front. In this study, PI controller tuning is simplified to a single-objective problem that minimizes ITAE, yielding the following objective function:

$$F_{objective} = a_1ITAE_1 + a_2ITAE_2 + \cdots + a_nITAE_n \quad (26)$$

This method enhances the system's dynamic response and overall control performance. To achieve optimal tuning, the GWO algorithm is employed due to its proven effectiveness in solving complex, multi-parameter optimization problems. The objective is to optimize the gains of eight PI controllers utilized within the system. Two of these controllers govern the boost converter in the wind generation unit, another two manage the bidirectional converter for the battery system, and the remaining four control the DC-AC converter. These controllers play a vital role in regulating active and reactive power flow as well as stabilizing both DC and AC voltage levels. The optimization focuses on tuning the proportional gains (K_{p1} to K_{p8}) and integral gains (K_{i1} to K_{i8}), ensuring the HDGS performs efficiently and reliably across diverse load and generation scenarios.

IV. Proposed Hybrid SPSO-DE Algorithm for PI Control Optimization

Optimization algorithms play a pivotal role in tuning PI controller parameters for microgrids, where system stability, fast dynamic response, and robustness are essential under varying generation and load conditions. Among the numerous metaheuristic methods, Particle Swarm Optimization (PSO) and Differential Evolution (DE) have been widely used for control parameter tuning due to their simplicity and effectiveness. However, each algorithm has inherent limitations that restrict their performance when applied individually. To overcome these drawbacks, this study introduces a hybrid algorithm that integrates Spherical Vector-Based PSO (SPSO)[68] with Differential Evolution (DE) [69] to enhance both global and local search capabilities. This hybrid framework synergistically combines the global search capabilities of Spherical Particle Swarm Optimization (SPSO) with the local search refinement of Differential Evolution (DE) to improve convergence speed, accuracy, and robustness in high-dimensional parameter spaces.

Particle Swarm Optimization (PSO) is a population-based stochastic optimization technique inspired by the social behaviour of birds and fish. In PSO, each particle represents a potential solution and flies through the search space by

adjusting its velocity and position based on its own best experience (personal best) and the swarm's best experience (global best). The velocity and position of each particle are updated using:

$$v_i^{t+1} = \omega v_i^t + c_1 r_1 (p_i^{best} - x_i^t) + c_2 r_2 (g^{best} - x_i^t) \quad (27)$$

$$x_i^{t+1} = x_i^t + v_i^{t+1} \quad (28)$$

where ω is the inertia weight, c_1 and c_2 are acceleration coefficients, and r_1, r_2 are random numbers in the range [0, 1]. Although PSO offers good convergence in the early search stage, it often suffers from premature convergence, especially in complex or multimodal problem spaces.

On the other hand, Differential Evolution (DE) is a robust and straightforward evolutionary algorithm designed for continuous optimization problems. It evolves a population by applying mutation, crossover, and selection operators. In the mutation step, a donor vector is generated by adding the weighted difference between two randomly selected individuals to a third one. Crossover then combines this donor vector with the current vector to produce a trial solution, and selection chooses the better of the two for the next generation. The standard mutation operation is expressed as:

$$V_i = X_{r1} + F.(X_{r2} - X_{r3}) \quad (29)$$

where X_{r1}, X_{r2}, X_{r3} are distinct individuals, and $F \in [0, 2]$ is the mutation scaling factor. DE is known for its simplicity and strong global search capability; however, it may require a large number of generations to fine-tune parameters locally and is sensitive to the choice of control parameters.

To harness the complementary strengths of both methods, this study proposes a Hybrid SPSO-DE algorithm. The foundation of this approach lies in enhancing the standard PSO by introducing spherical vector representation, allowing each particle's position to be defined in spherical coordinates—radial distance (ρ), polar angle (ξ), and azimuthal angle (ϕ). This spherical model enables better spatial exploration and prevents particles from converging prematurely along straight-line trajectories, which are common in Cartesian PSO.

In the Spherical PSO (SPSO) component, the particles update their velocities and positions using spherical motion equations. The update mechanism incorporates adaptive strategies for inertia weight and acceleration coefficients based on the current iteration and fitness performance. These adaptive parameters help balance exploration in the early stages and exploitation in later iterations. Furthermore, an additional acceleration term is included for particles that stagnate, boosting their ability to escape local optima.

Once the SPSO phase completes its velocity and position updates, the algorithm transitions to the DE phase, where selected elite or stagnated particles undergo mutation, crossover, and selection. By applying DE locally to high-potential solutions, the algorithm refines their positions, effectively enhancing precision near optimal regions. The integration of DE ensures that particles do not become trapped in sub-optimal areas and introduces diversity into the swarm, maintaining a healthy search dynamic.

To further improve convergence quality, the initial population in SPSO-DE is generated using a chaotic tent map with opposition-based learning (OBL). This dual-initialization approach ensures a well-dispersed and diverse set of solutions, reducing the likelihood of poor performance due to an ill-initialized swarm.

A. Spherical Particle Representation

Unlike traditional Cartesian-based PSO, the SPSO employs a spherical coordinate system to represent particles. Each particle μ_i^t is encoded as a triplet $(\rho_i^t, \xi_i^t, \phi_i^t)$, corresponding to radial distance, polar angle, and azimuthal angle, respectively. This representation is particularly advantageous for spherical problem spaces such as multivariable PI control surfaces in microgrids.

The velocity update in SPSO is expressed as:

$$\Delta\mu_i^{t+1} = \omega^t \Delta\mu_i^t + c_1^t r_{1,i} (P_{best,i}^t - \mu_i^t) + c_2^t r_{2,i} (G_{best}^t - \mu_i^t) + a_i^t \quad (30)$$

$$\mu_i^{t+1} = \mu_i^t + \Delta\mu_i^{t+1} \quad (31)$$

Where ω^t is inertia weight, adapted based on fitness variance, c_1^t, c_2^t is cognitive and social coefficients, dynamically modulated, $r_{1,i}, r_{2,i} \in [0,1]$ are random numbers, a_i^t is additional acceleration applied when particles stagnate.

The spherical positions are converted to Cartesian form for objective function evaluation:

$$x_{ix} = x_{(i-1)x} + \rho_{i-1} \cos\xi_{i-1} \cos\phi_{i-1} \quad (32)$$

$$x_{iy} = x_{(i-1)y} + \rho_{i-1} \cos\xi_{i-1} \sin\phi_{i-1} \quad (33)$$

$$x_{iz} = x_{(i-1)z} + \rho_{i-1} \sin\xi_{i-1} \quad (34)$$

B. Adaptive Mechanisms

To enhance dynamic control during optimization, adaptive mechanisms are introduced: Inertia weight ω^t is updated based on a fitness accuracy parameter fap^t:

$$\omega^t = \omega_{max} - (\omega_{max} - \omega_{min}).\frac{t}{T}.fap^t \quad (35)$$

Learning factors c_1^t and c_2^t vary nonlinearly over time:

$$x^t = \frac{1}{2}\sin\left(\frac{t}{T}\pi - \frac{pi}{2}\right) + \frac{1}{2} \quad (36)$$

$$c_1^t = c_{max} - (c_{max} - c_{min}) x^t fap^t \quad (37)$$

$$c_2^t = c_{min} + (c_{max} - c_{min}) x^t fap^t \quad (38)$$

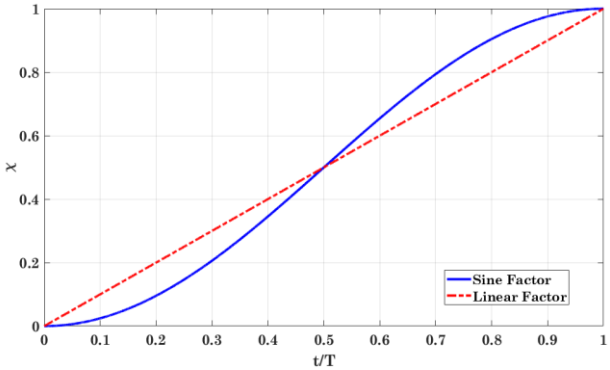

Fig. 8. Variation trends of learning factors during the iterative process

These adaptations ensure a balanced trade-off between exploration and exploitation during the search process. Figure 8 presents variation trends of learning factors during the iterative process.

C. Integration of Differential Evolution

To overcome stagnation and refine local search, a Differential Evolution (DE) strategy is integrated into the SPSO framework, particularly targeting the elite and stagnated particles. This integration proceeds through three primary operations:

1. Mutation:

$$V_i = \mu_{r1} + F.(\mu_{r2} - \mu_{r3}) \tag{39}$$

Where $\mu_{r1}, \mu_{r2}, \mu_{r3}$ are distinct randomly selected particles, and $F \in [0,2]$ is the scaling factor.

2. Crossover:

$$U_{i,j} = \begin{cases} V_{i,j}, & if\ rand_j \le CR\ or\ j = j_{rand} \\ \mu_{i,j} & otherwise \end{cases} \tag{40}$$

Where CR is the crossover probability

3. Selection:

$$\mu_i^{t+1} = \begin{cases} U_i, & if\ f(U_i) < f(\mu_i) \\ \mu_i, & otherwise \end{cases} \tag{41}$$

By embedding DE operations directly within the spherical framework, the proposed algorithm significantly improves the convergence behaviour, particularly in non-linear PI optimization landscapes.

D. Initialization Strategy

To maximize initial diversity and search efficacy, a tent chaotic map with perturbation is employed during initialization. This is complemented with opposition-based learning (OBL), where both original and opposite solutions are generated, and the best among them is retained based on fitness. This dual-stage initialization ensures robust global coverage and avoids premature convergence.

E. Enhanced Initialization Using Tent Map with Perturbation and Opposition-Based Learning

In conventional metaheuristic algorithms, the initialization of the population typically relies on the use of the standard pseudo-random number generator function, such as rand(). While simple and computationally efficient, such randomization methods often fail to provide a uniformly diverse distribution across the search space. This limited diversity in the early stages can significantly affect the convergence speed and global search capability of the algorithm. To overcome these shortcomings, the proposed hybrid SPSO-DE algorithm adopts a chaotic initialization technique based on the tent map, augmented with perturbation mechanisms, and further improved using opposition-based learning (OBL) [70].

The tent map is a deterministic chaotic map that generates sequences within the interval [0, 1] and is defined as follows:

$$\gamma_{t+1} = f_\psi(\gamma_t) = \begin{cases} \psi\gamma_t, & if\ \gamma_t < 0.5 \\ \psi(1-\gamma_t), & if\ \gamma_t \ge 0.5 \end{cases} \tag{42}$$

Here, ψ is a control parameter that influences the chaotic behavior of the system and is typically chosen within the range $(0, 2)$. When $\psi = 2$, the tent map reaches a fully chaotic regime, known as the central tent map, producing sequences with high randomness and coverage over [0, 1]. However, despite its chaos, the tent map may still suffer from small periodic cycles. For example, if $\gamma_t \in \{0.2, 0.4, 0.6, 0.8\}$, the sequence can become trapped in a loop. Furthermore, when γ_t equals specific values like 0.25, 0.5, or 0.75, the generated sequence may converge toward zero, leading to insufficient diversity in the initialized population as shown in figure 9.

To address these limitations, a perturbation strategy is introduced. The modified tent map with perturbation applies random corrections to break periodic cycles and avoid fixed-point convergence. The enhanced chaotic generator is defined as:

$$\gamma_{t+1} = f_\psi(\gamma_t) = \begin{cases} \psi_1\gamma_t + (2r_1 - 1), & 0 < \gamma_t < 0.5 \\ \psi_1(1-\gamma_t) + \frac{2r_2 - 1}{\psi_2}, & 0.5 < \gamma_t < 1 \\ r_3, & otherwise \end{cases} \tag{43}$$

In this formulation, r_1, r_2, r_3 are uniformly distributed random numbers in [0, 1] generated using $rand()$, while ψ_1 and ψ_2 are constants typically set to 2 and 100, respectively. These additional random perturbations ensure the generation of more scattered and non-repetitive values, thus promoting greater initial diversity and enhancing the exploration capability of the algorithm.

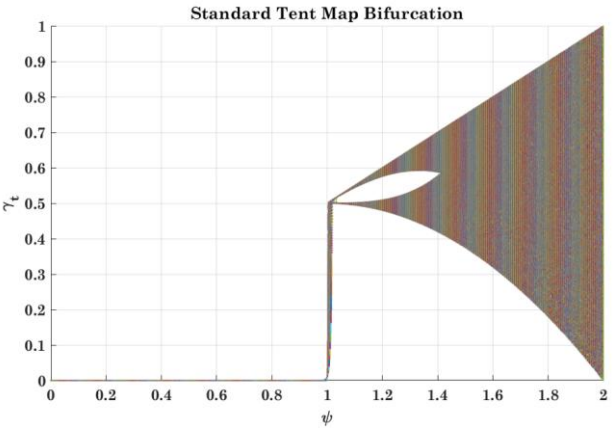

Fig. 9. Tent map under different parameters.

Once the chaotic sequence γ is generated using the perturbed tent map, it is mapped to the problem's decision space to initialize the search agents. For a search space defined by lower and upper bounds lb_i and ub_i, the initial position of each agent is calculated as:

$$X_{j,i}^0 = lb_i + (ub_i - lb_i).\gamma \tag{44}$$

where j denotes the j-th particle and i denotes the i-th dimension of the problem. This transformation ensures that all initialized particles are uniformly distributed within their respective search space limits.

To further improve the initialization quality and accelerate convergence, the method incorporates Opposition-Based Learning (OBL). Instead of relying solely on the current solution, OBL simultaneously generates an opposite solution for each agent. The opposite solution for each dimension is calculated using:

$$X'^{0}_{j,i} = lb_i + ub_i - x^0_{j,i} \quad (45)$$

This approach doubles the candidate pool by producing both an initial solution and its corresponding opposite, forming a combined set of $2b$ agents, where b is the number of particles in the population. These $2b$ agents are evaluated based on the objective function, and the top b solutions with the best fitness values are retained as the final initialized population.

By integrating chaotic initialization with perturbation and OBL, the proposed strategy significantly enhances the diversity, uniformity, and coverage of the initial search space. This diverse initial population helps the SPSO-DE algorithm avoids premature convergence and local optima while accelerating the convergence rate. The dual-layer randomness introduced by chaotic dynamics and the balance offered by opposition-based reflection together ensure a strong foundation for the algorithm's subsequent optimization phases.

F. Algorithm Summary

The SPSO-DE algorithm proceeds as follows:

1. Initialize particles using chaotic tent map and OBL.
2. Evaluate objective fitness
3. For each iteration:
   - Update inertia and learning factors adaptively.
   - Update particle positions using SPSO equations.
   - Apply DE operations to elite or stagnated particles.
   - Evaluate and select best solutions.
   - Update personal and global best positions.
4. Terminate upon convergence or maximum iterations.

V. SIMULATION RESULTS

This section presents the simulation results used to evaluate the effectiveness of the proposed Hybrid Spherical Vector Particle Swarm Optimization–Differential Evolution (HSPSO-DE) control strategy. All simulations were performed in MATLAB/Simulink, with the system parameters summarized in Table 1. To objectively assess performance, HSPSO-DE is benchmarked against three widely adopted optimization techniques: Genetic Algorithm (GA) [23], Particle Swarm Optimization (PSO) [24], and Grey Wolf Optimizer (GWO) [25]. The control architecture described in Section 3 is applied to the microgrid configuration shown in Figure 1, and the PI controller gains optimized by each algorithm are listed in Table 2. The system's dynamic response is evaluated under three representative operating conditions: (1) variations in irradiance, temperature, and wind speed; (2) step changes in reference power; and (3) fluctuations in load demand. Figure 10(a) illustrates the active power tracking performance, where HSPSO-DE demonstrates noticeably faster response and reduced tracking error compared to GA, PSO, and GWO. Similarly, Figure 10(b) shows the DC-link voltage regulation, confirming that HSPSO-DE maintains tighter voltage control throughout transient disturbances. Table 2 provides a summary of the optimized PI gains, while Table 3 presents the comparative performance indices, clearly showing that the proposed hybrid optimization method outperforms the conventional algorithms reported in the literature.

TABLE I. PARAMETERS OF THE HYBRID DG SYSTEM

Parameter	Value
PV Array	
Manufacturer and Model	LG, LG350N2W-B3
Open Circuit Voltage (V_{oc})	48.1 V
Short Circuit Current (I_{sc})	9.74 A
Maximum power point voltage (V_{mpp})	37.9 V
Maximum power point current (I_{mpp})	9.24 A
Series-connected modules per string	43
Parallel strings	10
PMSG	
Stator Resistance	0.8634
Stator Inductance	0.8121 µH
Torque Constant	4.82
Inertia	0.0027
Wind Turbine	
Mechanical output power	150 kW
Base wind speed	11 m/s
Rotor diameter	24.5 m
Swept rotor area	480 m2
Battery	
Nominal voltage	600
Rated capacity	800
Grid	***11 kV, 50 Hz***

A. Case 1: Analysis of Irradiance, Temperature, and Wind Speed Variations

Case 1 examines the dynamic behavior of the proposed HSPSO-DE–based PI control strategy under fluctuating environmental conditions. Since real-world microgrids frequently operate under unpredictable solar and wind patterns, this scenario provides a realistic assessment of the system's capability to maintain stability, power balance, and power quality. MATLAB/Simulink is used to simulate a 20-second operating period during which irradiance, temperature, and wind speed are deliberately varied to introduce nonlinearity and stress the hybrid renewable energy system. The irradiance and temperature profiles used in the simulation are shown in Figure 11(a). These conditions are intentionally chosen to represent typical daytime variations that a microgrid may encounter. From 0 to 4 seconds, solar irradiance is maintained at a low value of 200 W/m² with a temperature of 30°C, representing early morning conditions. Between 4 and 8 seconds, irradiance gradually increases to 400 W/m² and temperature rises to 32°C. A further increase is introduced between 8 and 12 seconds, where irradiance reaches 600 W/m² and temperature rises to 34°C. From 12 to 20 seconds, the irradiance profile progresses through 800 W/m² at 36°C until it reaches a peak of 1000 W/m² at 38°C. These meticulously constructed test intervals introduce nonlinear changes that challenge the system's ability to track the maximum power point and regulate converter outputs

efficiently. Simultaneously, wind speed variations are applied to stress-test the wind energy conversion system. The wind profile begins at 8 m/s from 0 to 3 seconds, followed by an increase to 9 m/s between 3 and 6 seconds. Wind speed further increases to 10 m/s during 6–8 seconds and then reaches 11 m/s between 8 and 12 seconds. The peak speed of 12 m/s is applied from 12 to 15 seconds. Afterward, wind speed decreases to 10 m/s between 15 and 18 seconds and drops to 8 m/s at the end of the simulation. These variations closely emulate real atmospheric patterns and allow assessment of the system's response to both rising and falling wind levels.

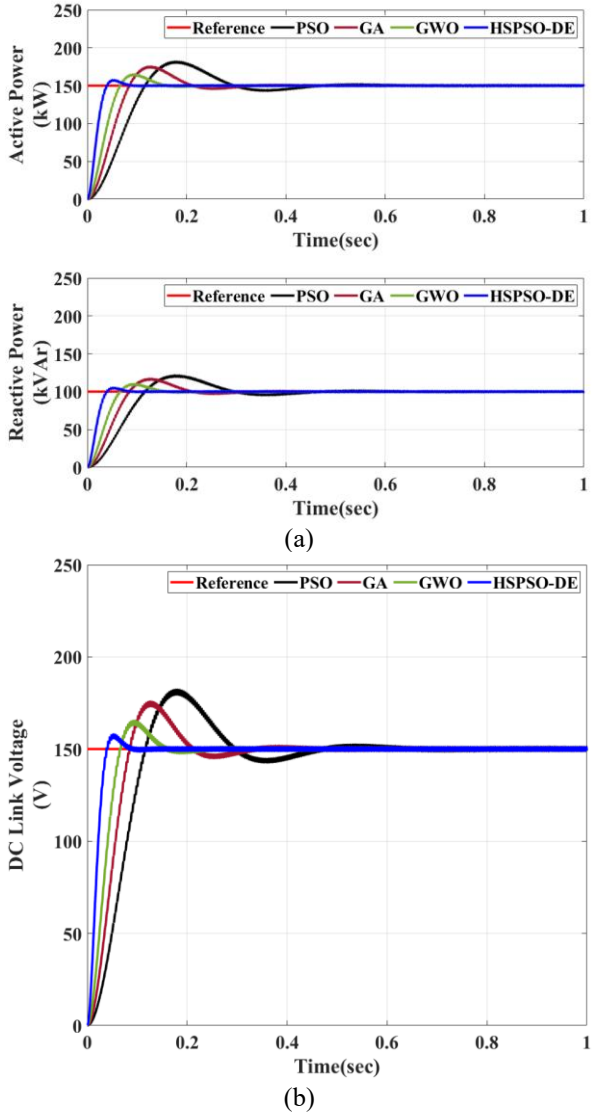

Fig. 10. (a) power tracking performance (b) DC bus voltage tracking performance

Figure 11(b) presents the corresponding PV and wind power generation curves. As expected, PV power increases as irradiance intensifies and temperature rises. The MPPT algorithm ensures that the PV system tracks the changing maximum power point effectively, resulting in a smooth upward trend in power output. Similarly, wind power is strongly correlated with wind speed, demonstrating increased generation during peak wind periods and reductions as wind speed declines.

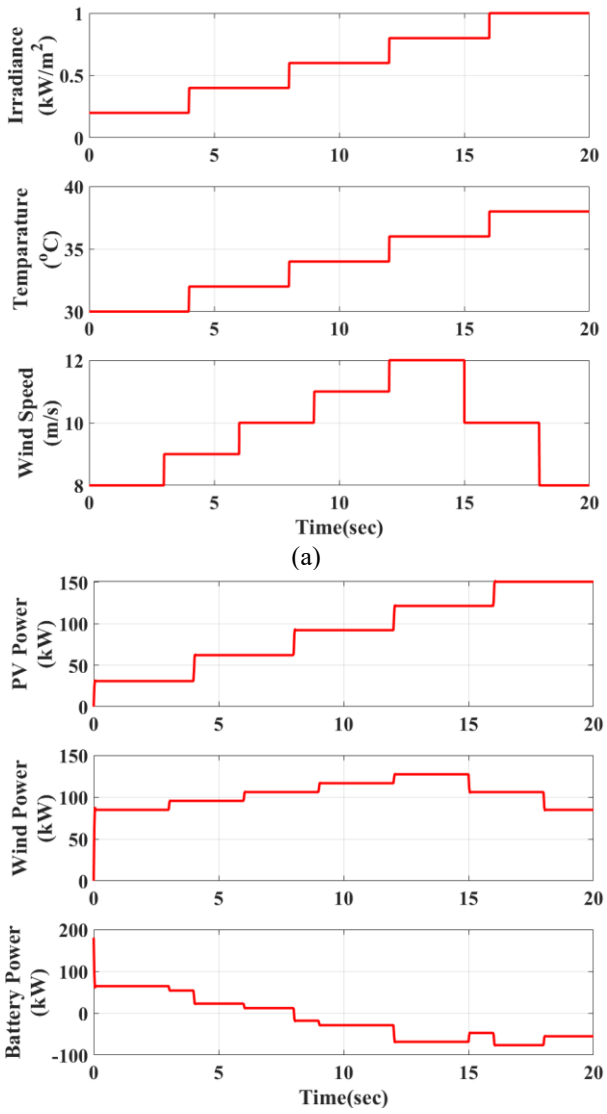

Fig. 11. (a) Irradiance, temperature input to the PV system and wind speed input to the wind generation system (b) generated power from PV, wind and terminal power of the battery

The close alignment between environmental profiles and generation curves confirms that both renewable subsystems operate reliably under fluctuating conditions. The battery energy storage system (BESS) plays a critical stabilizing role in this hybrid architecture. During the early portion of the simulation (0–8 seconds), renewable generation is insufficient to satisfy the power demanded by the Voltage Source Converter (VSC). As a result, the battery discharges to compensate for the deficit. This behavior is reflected as positive battery power values, indicating energy flow from the battery into the DC link. As irradiance and wind speed progressively increases beyond 8 seconds, the renewable power surpasses the VSC's reference requirements, and the battery shifts into charging mode. The negative power values recorded during this period reflect energy absorption by the BESS.

TABLE II. OPTIMIZED PI CONTROLLER GAINS OBTAINED USING THE PROPOSED ALGORITHM AND OTHER COMPARATIVE OPTIMIZATION TECHNIQUES.

Algorithm	K_{p1}, K_{i1}	K_{p2}, K_{i2}	K_{p3}, K_{i3}	K_{p4}, K_{i4}	K_{p5}, K_{i5}	K_{p6}, K_{i6}	K_{p7}, K_{i7}	K_{p8}, K_{i8}
Proposed HSPSO-DE	0.9654 6.1387	1.6785 5.2374	1.0257 1.7628	1.9344 2.6819	0.3781 1.6637	0.8270 2.5192	1.7029 3.1578	1.4691 3.5284
GWO	0.8221 5.9568	1.8265 4.4410	0.9588 1.0731	1.7920 2.2863	0.2962 1.4625	1.0033 1.4135	0.9098 2.5126	0.5197 2.2459
PSO	0.4517 7.9595	2.1464 5.1731	0.7417 1.0570	1.6142 2.6405	0.1328 1.5571	0.7457 2.4346	1.5295 1.9126	1.1673 1.9816
GA	0.6283 7.3236	2.0684 5.0611	0.7837 1.6274	1.0361 2.5383	0.3039 1.8097	0.49590 2.09410	1.6852 2.9816	1.3414 2.7502

TABLE III. PERFORMANCE INDICES COMPARISON

Algorithm	DC Bus Voltage				Active Power				Reactive Power			
	IAE	*ISE*	*ITAE*	*ITSE*	*IAE*	*ISE*	*ITAE*	*ITSE*	*IAE*	*ISE*	*ITAE*	*ITSE*
Proposed HSPSO-DE	0.02833	0.01487	0.0085	0.006674	0.0319	0.0248	0.007395	0.001833	0.02274	0.01729	0.00653	0.00721
GWO	0.0514	0.0279	0.0167	0.01264	0.0598	0.0477	0.0149	0.0037	0.0451	0.0342	0.0135	0.0146
PSO	0.0456	0.0212	0.0213	0.0056	0.0353	0.0354	0.0028	0.0037	0.0381	0.01827	0.01588	0.01957
GA	0.04881	0.03369	0.01573	0.01690	0.04378	0.03715	0.01100	0.00872	0.04631	0.02157	0.01105	0.01088

Figure 14 shows the evolution of battery State of Charge (SOC), capturing these transitions clearly. SOC decreases during early discharging periods and gradually increases when charging begins, demonstrating the battery's successful contribution to system balancing. The VSC is responsible for maintaining regulated active and reactive power outputs at the AC side of the microgrid.

For this case, the VSC reference values are fixed at 150 kW (active) and 100 kVAR (reactive), as illustrated in Figure 12(a). Maintaining these values is essential for ensuring stable power delivery. Despite the fluctuating generation from PV and wind and the varying charging/discharging behavior of the battery, Figure 12(b) confirms that the VSC successfully tracks these reference values throughout the full 20-second period.

This performance directly demonstrates the effectiveness of the HSPSO-DE–optimized PI controller, whose optimized gains allow rapid transient response and robust tracking capability under disturbances. While the VSC contributes a significant portion of the load demand, it does not supply the entire microgrid requirement. The total load connected during this case requires 250 kW of active power and 120 kVAR of reactive power. Since the VSC provides only its 150 kW and 100 kVAR reference values, the remaining imbalance is compensated by importing power from the utility grid. Figure 13(a) shows the active and reactive power drawn from the grid, confirming smooth transitions between grid import levels as renewable supply and battery charging conditions evolve. The absence of sharp variations or instability indicates that the proposed control method successfully coordinates renewable generation, battery assistance, and grid support.

Maintaining a stable DC link voltage is crucial for proper converter operation and overall microgrid stability. Figure 13(b) compares the actual DC link voltage with its reference value. Despite the substantial fluctuations in generation and battery behavior, the proposed scheme maintains tight voltage regulation throughout the simulation. This demonstrates the robustness of the HSPSO-DE–optimized PI controller in handling nonlinearities and disturbance-induced voltage deviations.

Beyond stability and power balancing, power quality remains an essential evaluation metric. Figures 15(a)–15(c) present the Total Harmonic Distortion (THD) levels of the load current, VSC current, and grid current. The THD values measured—1.99% for the load current, 1.94% for VSC current, and 1.28% for grid current—are significantly lower than the IEEE 519 standard limits. These results confirm that the proposed method not only stabilizes power flows but also ensures high-quality waveforms under dynamic operation.

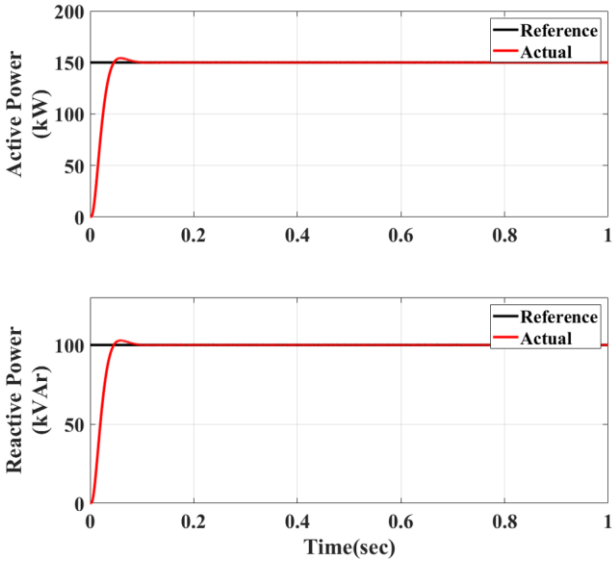

(a)

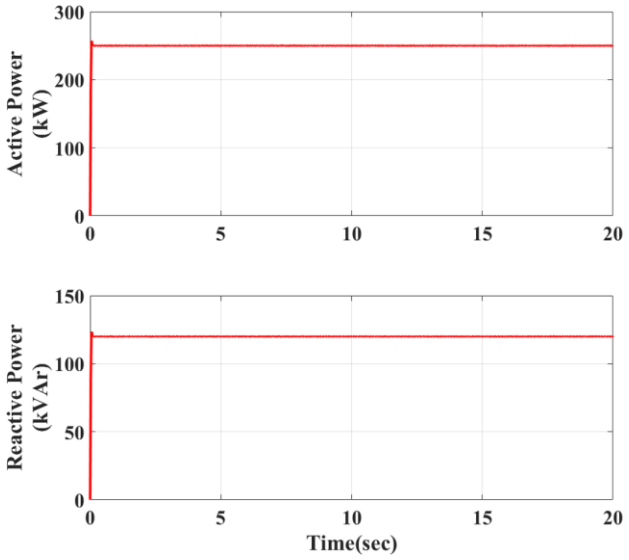

(b)

Fig. 12. (a) Reference and actual active and reactive power converted by the VSC (b) Load active and reactive powers

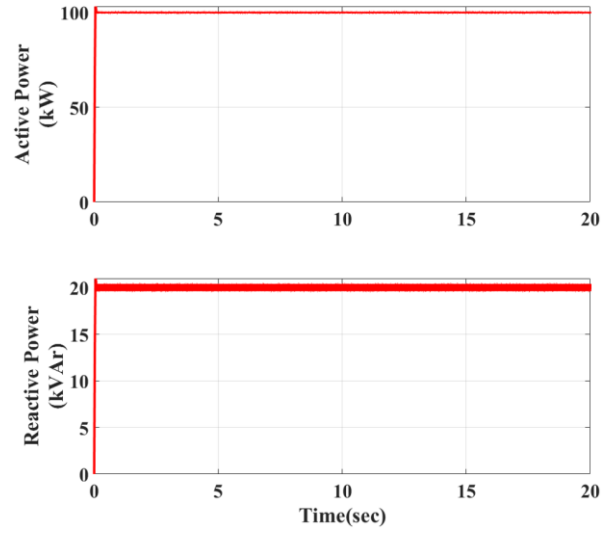

(a)

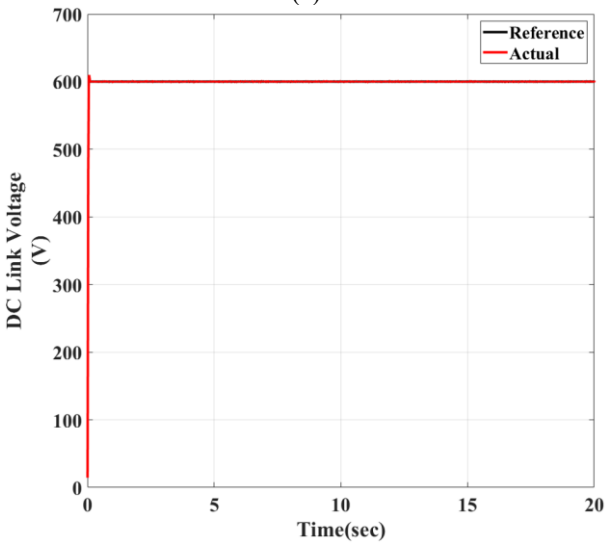

(b)

Fig. 13. (a) Active and reactive powers provided by the grid (b) DC Link Voltage

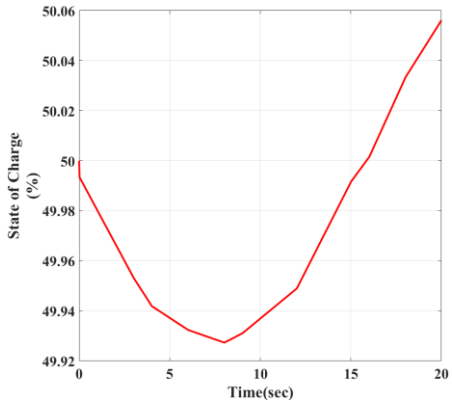

Fig. 14. State of charge of the battery in %

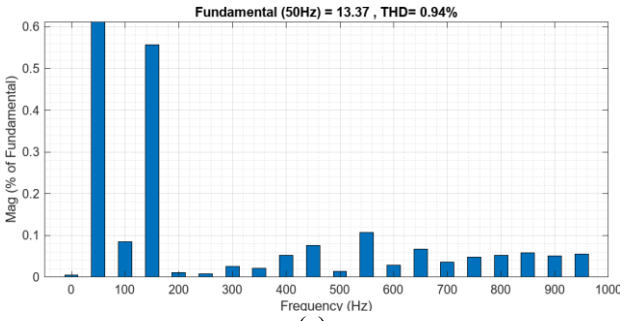

(a)

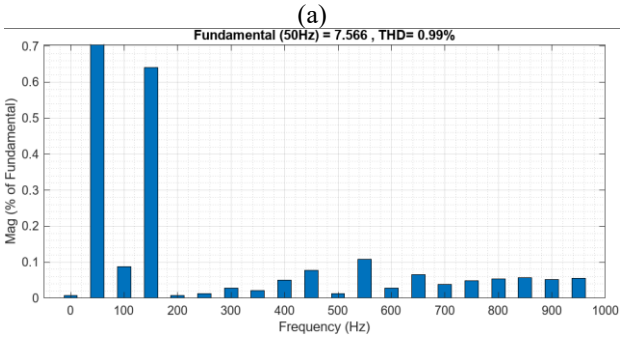

(b)

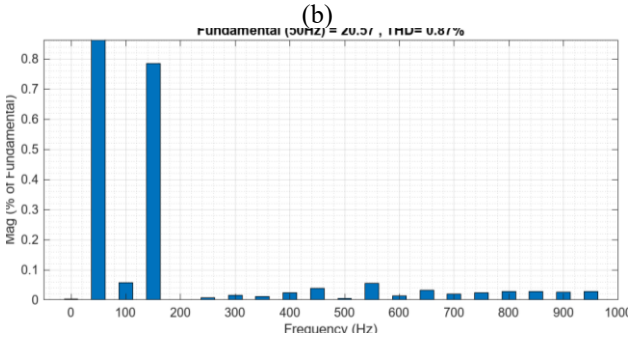

(c)

Fig. 15. (a) load current (b) VSC current and (c) grid current THDs

B. Case 2: Analysis of reference active and reactive power variations

This simulation case is designed to evaluate the dynamic response and effectiveness of the HSPSO-DE-optimized PI controller in managing variations in the reference active and reactive power inputs to the Voltage Source Converter (VSC), under constant environmental conditions. By maintaining fixed irradiance and wind speed, the influence of renewable energy fluctuations is eliminated, allowing the performance of the control system to be assessed solely based on its response to deliberate reference signal changes.

In this scenario, the irradiance is held constant at 800 W/m², and the wind speed remains steady at 11 m/s throughout the 20-second simulation period. These conditions, depicted in Figure 16(a), ensure that the power output from both the photovoltaic (PV) array and the wind turbine remains stable. This steady renewable generation enables a clear evaluation of how effectively the battery energy storage system and the VSC respond to step changes in the power demand set points.

Figure 16(b) presents the power outputs from the PV and wind systems along with the battery's contribution. Since the renewable energy inputs are constant, the battery dynamically adjusts its operation—switching between charging and discharging—to compensate for the difference between the fixed renewable supply and the varying VSC power reference values. The reference values for active and reactive power are altered in multiple steps during the simulation to assess controller performance under a range of load conditions. The sequence of changes is as follows:

- **0–3 seconds:** 60 kW active power and 30 kVAR reactive power,
- **3–6 seconds:** 150 kW and 150 kVAR,
- **6–9 seconds:** 220 kW and 200 kVAR,
- **9–12 seconds:** 350 kW and 320 kVAR,
- **12–15 seconds:** 400 kW and 160 kVAR,
- **15–18 seconds:** 200 kW and 150 kVAR,
- **18–20 seconds:** 100 kW and 40 kVAR.

These changes simulate different operational demands, reflecting the dynamic load profiles that a microgrid controller must handle in real-time applications.

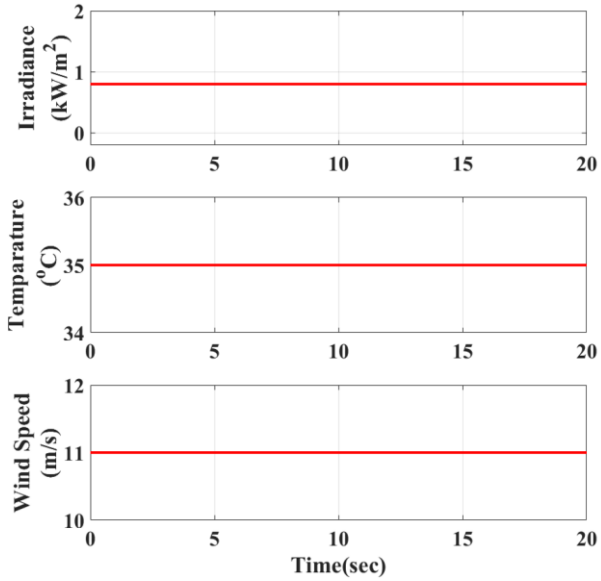

(a)

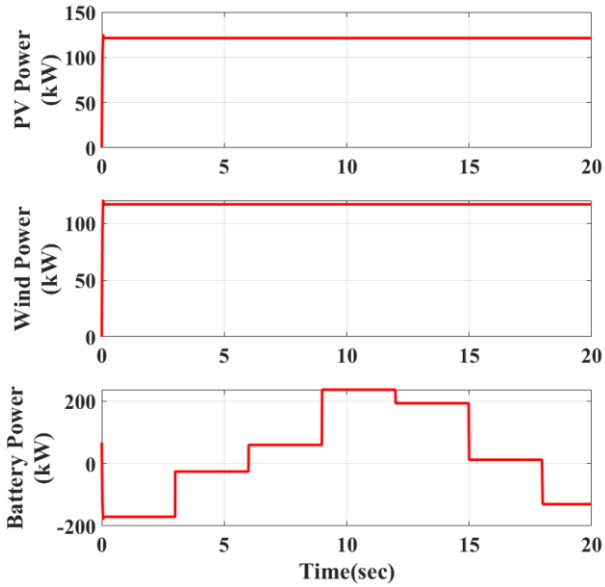

(b)

Fig. 16. (a) Irradiance, temperature input to the PV system and wind speed input to the wind generation system (b) generated power from PV, wind and terminal power of the battery

When the reference power values are lower than the available renewable energy (e.g., from 0–6 seconds and after 18 seconds), the surplus energy is directed to the battery storage, resulting in charging behavior. Conversely, during periods where the reference power exceeds the combined renewable generation—particularly between 6 and 18 seconds—the battery transitions into discharging mode, supplying the deficit. This transition between modes is smooth and well-regulated, showcasing the adaptability of the proposed HSPSO-DE-based control strategy.

Figure 17(a) illustrates the actual versus reference active and reactive power delivered by the VSC. The response shows a close match between the actual and target values, indicating precise tracking performance of the controller. The ability of the PI controller, tuned using the HSPSO-DE algorithm, to follow rapid step changes in power demand with minimal overshoot and steady-state error underlines the robustness of the optimization approach.

Figure 17(b) highlights the load demand, which remains within a fixed range. Since the VSC output sometimes exceeds the load requirement, the surplus power is exported to the utility grid. Figure 18(a) illustrates this back-feed to the grid, confirming that the system can not only meet internal power requirements but also effectively manage excess energy by exporting it—an important aspect for grid-connected microgrids aiming at bidirectional power flow capability.

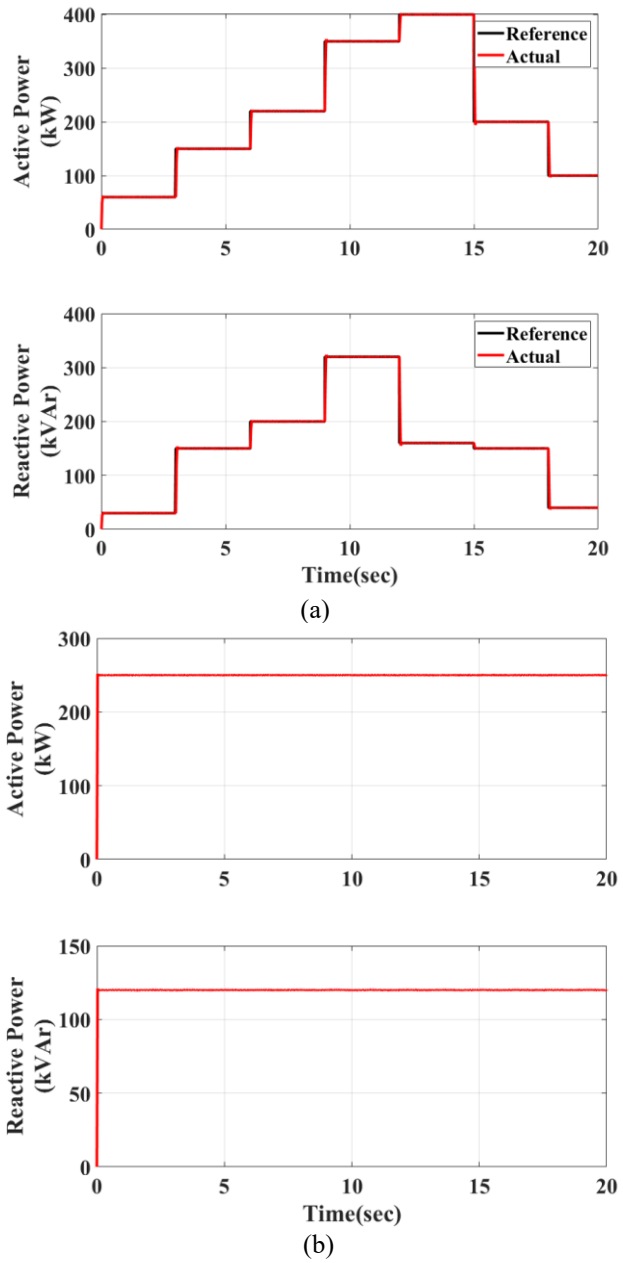

Fig. 17. (a) Reference and actual active and reactive power converted by the VSC (b) Load active and reactive powers

The battery's State of Charge (SOC), as shown in Figure 18(b), reflects the dynamic balance of power in the system. Between 6 and 18 seconds—when the system experiences a power shortfall—the battery discharges to meet the high reference demands, causing the SOC to decrease. In contrast, during intervals of power surplus, the battery enters charging mode, leading to an increase in SOC. This pattern confirms that the energy storage system is being utilized efficiently and is essential for buffering the system during periods of power mismatch.

In summary, Case 2 clearly demonstrates the capability of the HSPSO-DE-tuned PI controller to adapt to abrupt variations in power reference values. By maintaining constant environmental conditions, the effectiveness of the proposed control strategy in managing internal energy flow is isolated and validated. The system responds reliably to changes in power demand, with the battery storage effectively smoothing power imbalances and the VSC achieving high-fidelity tracking of the reference values. Moreover, the system's ability to export excess energy to the grid and maintain stable battery operation further highlights the intelligence and efficiency of the proposed control framework. These results reinforce the potential of the HSPSO-DE algorithm in ensuring optimal and reliable microgrid operation under dynamic load conditions.

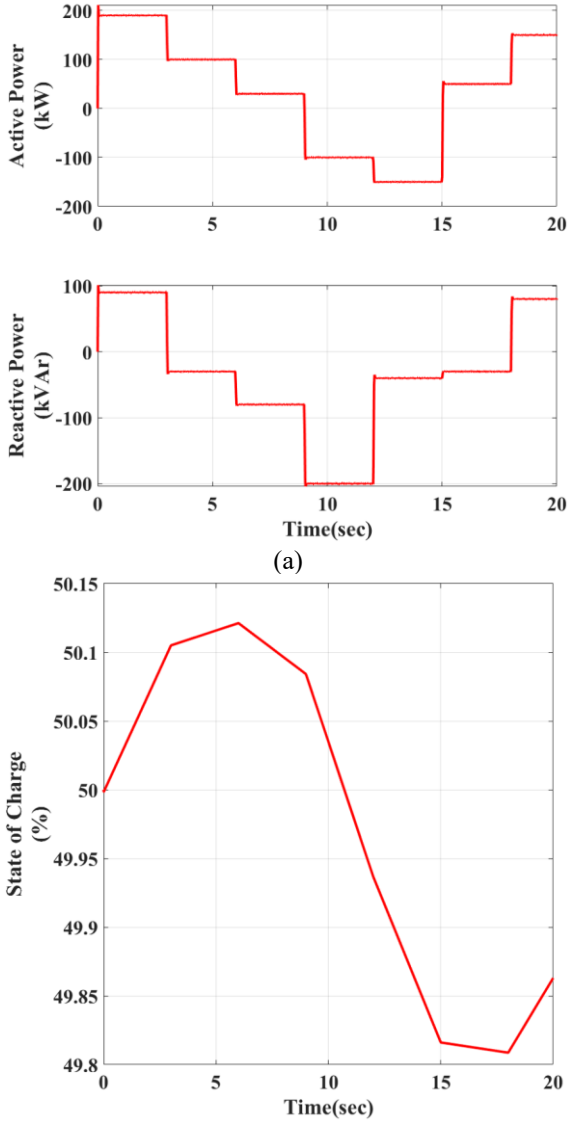

Fig. 18. (a) Active and reactive powers provided by the grid (b) SOC of the battery in %

C. *Case 3: Analysis of Load Variation and System Response*

This simulation scenario explores the response of the proposed hybrid renewable energy system—optimized using the HSPSO-DE-tuned PI controller—under varying load conditions, while maintaining constant generation parameters. The objective is to assess the system's capability to maintain power balance and operational stability when faced with dynamic load demands.

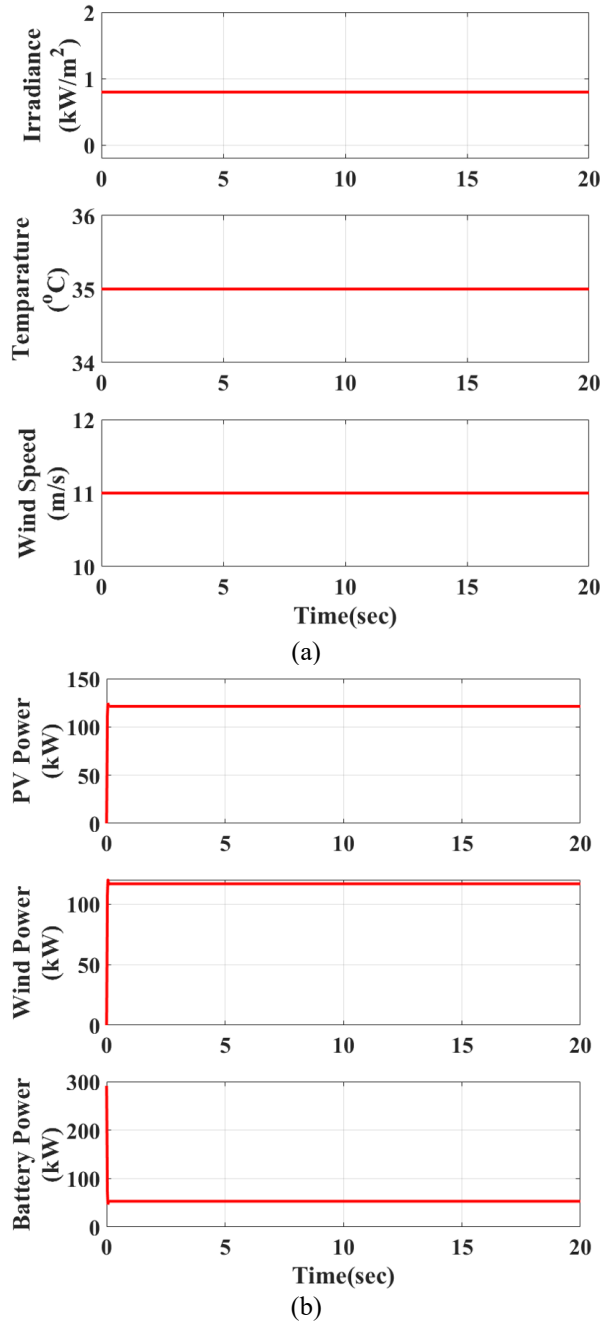

Fig. 19. (a) Irradiance, temperature input to the PV system and wind speed input to the wind generation system (b) generated power from PV, wind and terminal power of the battery

Throughout this simulation, the environmental conditions are kept unchanged. The irradiance remains fixed at 800 W/m², the temperature at 36°C, and the wind speed at a steady 11 m/s. These stable conditions ensure that the power output from the photovoltaic (PV) array and the wind turbine stays constant, as shown in Figures 19(a) and 19(b). This setup isolates the impact of load variation from renewable fluctuations, allowing for a focused analysis of how the control system manages demand-side changes.

In this case, the reference active and reactive power for the Voltage Source Converter (VSC) are held constant at 150 kW and 140 kVAr, respectively. These values define the fixed power delivery expected from the VSC to the load, regardless of the actual load demand. This constant reference enables the VSC to act as a stable source, and its performance in maintaining output under varying demand conditions can be critically evaluated.

The load undergoes several variations during the 20-second simulation. As illustrated in Figure 20(a), the active and reactive power requirements of the load change as follows:

- **0–3 seconds:** 50 kW and 40 kVAr,
- **3–6 seconds:** 120 kW and 90 kVAr,
- **6–9 seconds:** 180 kW and 120 kVAr,
- **9–12 seconds:** 250 kW and 240 kVAr,
- **12–15 seconds:** 300 kW and 250 kVAr,
- **15–18 seconds:** 220 kW and 190 kVAr,
- **18–20 seconds:** 200 kW and 180 kVAr.

This profile simulates realistic load fluctuations in a grid-connected microgrid and provides a suitable basis to test the system's responsiveness and flexibility. Despite these variations in load demand, the VSC continues to deliver power at the constant reference values of 150 kW and 140 kVAr. As shown in Figure 20(b), the actual power consumed by the load diverges from the VSC's output, creating a power mismatch that the system must address in real-time. This is managed through dynamic power exchange with the utility grid, as illustrated in Figure 21(a). When the load requires more power than what the VSC supplies—such as between 6 and 18 seconds—the grid supplements the deficit. Conversely, when the load demand is lower than the VSC's output—particularly in the early and final stages of the simulation—the excess power is exported to the grid.

This seamless exchange between the system and the grid ensures continuous power supply to the load while keeping the VSC operating at its set reference levels. It also reflects the system's bidirectional power handling capability, which is critical for smart microgrids aiming for flexibility, reliability, and efficient energy distribution.

Meanwhile, the battery's State of Charge (SOC) is closely tied to the overall energy balance. As the combined power output from the PV and wind systems exceeds the fixed VSC reference values, the surplus energy that is not consumed by the load or exported to the grid is directed toward charging the battery. Figure 21(b) shows the progressive increase in SOC over the simulation period, confirming that the battery remains in charging mode throughout this case. The system effectively captures excess energy and stores it for future use, enhancing overall efficiency and reducing dependency on the grid during high demand periods.

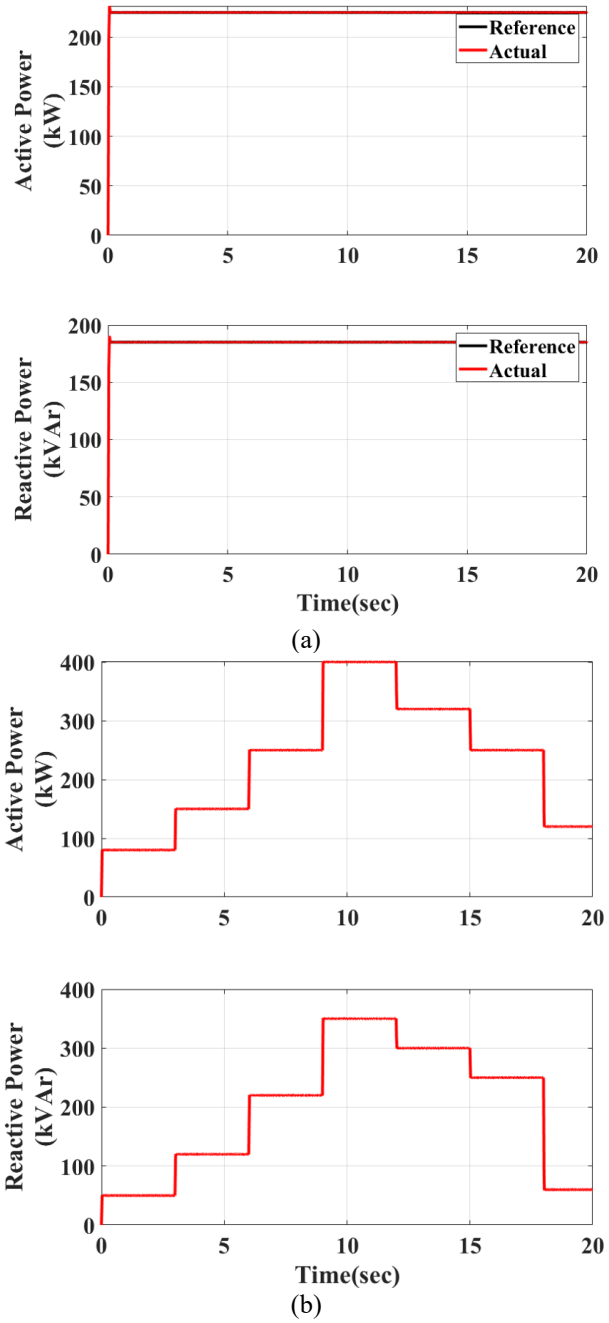

Fig. 20. (a) Reference and actual active and reactive power converted by the VSC (b) Load active and reactive powers

The results from Case 3 highlight the resilience and coordination within the hybrid energy system. Despite the fluctuations in load demand, the control system, enabled by HSPSO-DE-optimized PI gains, ensures stable power delivery from the VSC. The grid acts as a reliable buffer, compensating for any mismatch between generation and consumption, while the battery operates intelligently to absorb surplus power. This cooperative functioning of the generation units, energy storage system, and the grid ensures a robust and adaptive power management scheme. Overall, this case illustrates that under constant renewable generation, the system is well-equipped to handle dynamic load profiles without compromising stability or efficiency. The proposed control strategy maintains consistent VSC operation, enables efficient grid integration, and optimizes energy usage through intelligent battery management, which validates the effectiveness of the HSPSO-DE-based control approach in real-world microgrid applications.

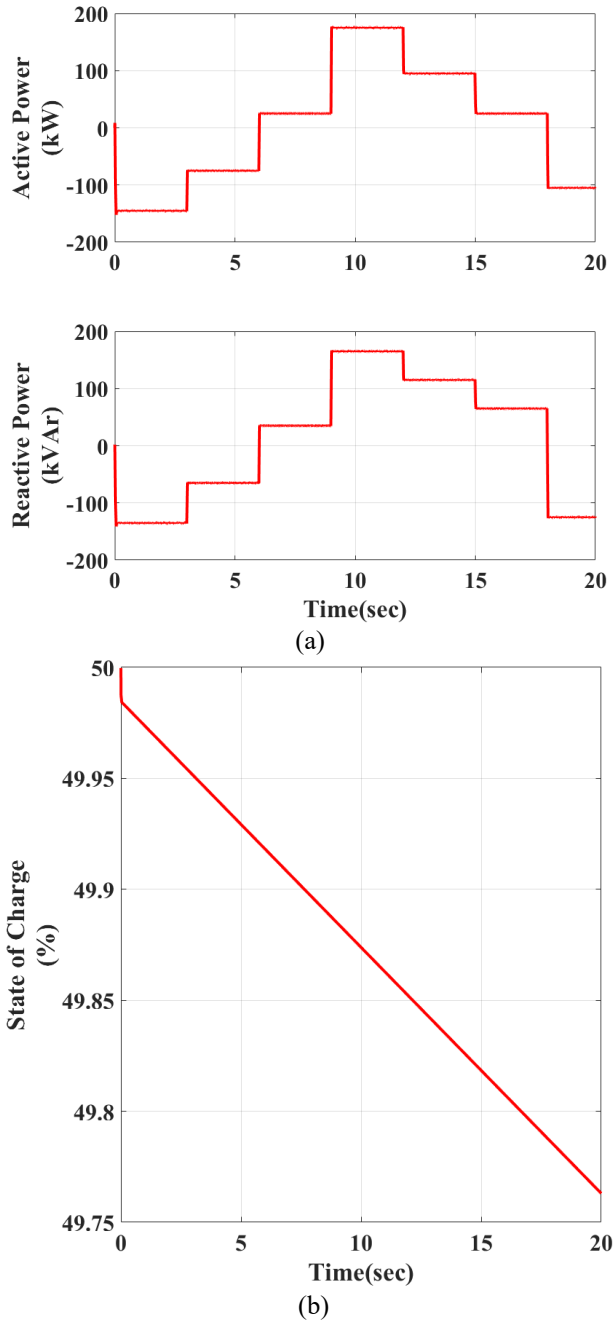

Fig. 21. (a) Active and reactive powers provided by the grid (b) State of charge of the battery in %

VI. CONCLUSION

This study proposed a Hybrid Spherical Vector Particle Swarm Optimization–Differential Evolution (HSPSO-DE) algorithm for the optimal tuning of PI controller gains in a renewable-integrated microgrid consisting of photovoltaic (PV), wind, and battery energy storage systems. Across three representative simulation scenarios—environmental variations, dynamic changes in reference power, and fluctuating load demand—the HSPSO-DE–optimized control strategy consistently demonstrated improved performance relative to benchmark algorithms such as GA, PSO, and

GWO. The hybrid approach achieved faster transient response, reduced steady-state error, better DC-link voltage regulation, lower Total Harmonic Distortion (THD), and more balanced utilization of storage resources. These outcomes collectively validate the effectiveness of combining spherical-vector exploration with DE-based exploitation for robust control in nonlinear microgrid environments. A key theoretical contribution of this work lies in establishing the value of spherical vector representation for high-dimensional control optimization. Traditional Cartesian PSO often suffers from axis-aligned stagnation and reduced directional diversity, which limits its ability to navigate complex landscapes involving multiple interacting PI parameters. By contrast, spherical-vector PSO decomposes particle motion into magnitude and directional components, enabling richer exploration and improved adaptability to nonlinearities. When integrated with the strong local refinement capability of DE, the proposed HSPSO-DE algorithm forms a geometry-aware optimization framework well suited for converter-level microgrid control. Beyond algorithmic performance, the study provides broader insight into coordinated operation within hybrid microgrids. In all cases, the PI-controlled Voltage Source Converter (VSC) successfully maintained active and reactive power references despite disturbances. The battery system dynamically modulated its charging and discharging behavior in response to renewable variability, ensuring continuous power balance and improved system resilience. The interaction between renewable subsystems, storage, VSC, and the utility grid was stable and efficient, reflecting the practical relevance of the proposed strategy for real-world microgrid architecture. However, the study also presents several limitations that should guide future work. First, the results are based entirely on simulation; hardware-in-the-loop (HIL) or physical prototype validation is essential to assess practical feasibility, real-time computational requirements, and controller robustness under sensor noise and switching distortions. Second, although the hybrid algorithm performed well, its scalability to larger microgrids with multiple converters or multi-microgrid clusters remains unexplored. Third, sensitivity to hyperparameters—such as population size, mutation factors, and weighting coefficients—was not systematically evaluated, and the absence of multi-run statistical analysis limits the strength of claims regarding repeatability and convergence reliability. Finally, although the algorithm shows strong performance in the tested scenarios, generalizing these results to all operating conditions requires cautious interpretation. Despite these constraints, the findings emphasize that geometry-enhanced hybrid optimization can substantially improve PI controller performance in renewable-rich microgrids. The HSPSO-DE framework provides a promising foundation for advanced control strategies that can adapt to increasing renewable penetration and operational uncertainty. Future research will focus on several directions. Hardware or HIL validation will be conducted to confirm real-time applicability; statistical benchmarking across multiple independent runs will be performed to quantify variability and robustness; and hyperparameter sensitivity studies will be added to strengthen confidence in the algorithm's stability. Extending the approach to multi-converter coordination, microgrid clusters, and demand-side response, as well as integrating cybersecurity-aware control mechanisms, will further enhance the applicability of the proposed method. This study contributes new knowledge by demonstrating how a geometry-aware hybrid metaheuristic can address long-standing challenges in PI controller tuning for hybrid microgrids, offering both theoretical advancement and practical potential for future renewable energy systems..

REFERENCES

[1] Adebayo, Damola Habeeb, Joshua Adenrele Ajiboye, Ugochukwu Daniel Okwor, Aminu Labaran Muhammad, Chikadibia Daniel Ugwuijem, Emmanuel Kenechukwu Agbo, and Victor Ikechukwu Stephen. "Optimizing energy storage for electric grids: Advances in hybrid technologies." *management* 10 (2025): 11.

[2] Ibitoye, O. T., Onibonoje, M. O., & Dada, J. O. (2023). Analysis of Power Quality and Technical Challenges in Grid-Tied Renewable Energy. *Europe*, *575*(608), 647.

[3] Andrade, I., Pena, R., Blasco-Gimenez, R., Riedemann, J., Jara, W. and Pesce, C., 2021. An active/reactive power control strategy for renewable generation systems. *Electronics*, *10*(9), p.1061.

[4] Chen, Keng, James Garrett, Kang Peng, Ronald Hulfachor, and Marvin Onabajo. "Buck circuit design with pseudo-constant frequency and constant on-time for high current point-of-load regulation." *IEEE Transactions on Circuits and Systems I: Regular Papers* 68, no. 10 (2021): 4062-4075.

[5] Shaija, P. J., and Asha Elizabeth Daniel. "Optimal tuning of PI controllers for IM drive using GWO and TLBO algorithms." In *2023 Fifth International Conference on Electrical, Computer and Communication Technologies (ICECCT)*, pp. 01-09. IEEE, 2023.

[6] Balasani, Srinivasa Rao, T. Santhana Krishnan, P. Venkata Prasad, and Leeth Hassen Jaseem. "Integration of Solar Photovoltaic with Modular Multiport Converter Using a Pi Controller Optimized Through Hybrid Osprey Optimization Algorithm and Relational Bi-Level Aggregation Graph Network." *International Journal of Computational Intelligence and Applications* (2025): 2450036.

[7] MANDAL, BARUN, Satabdi Chatterjee, Provas Roy, and Indranil Mukherjee. "A novel evolutionary algorithm named oppositional based chaotic tree seed algorithm (OCTSA) applied for energy cost minimization in hybrid microgrid system for different locations in India." (2023).

[8] Zulu, Musawenkosi Lethumcebo Thanduxolo, Rudiren Pillay Carpanen, and Remy Tiako. "A comprehensive review: study of artificial intelligence optimization technique applications in a hybrid microgrid at times of fault outbreaks." *Energies* 16, no. 4 (2023): 1786.

[9] Li, Ping, and Qian Liu. "Optimizing energy management strategies for microgrids through chaotic local search and particle swarm optimization techniques." *Heliyon* 10, no. 17 (2024).

[10] Zhang, Xiaowen, Shuqing Zhang, Wei Dong, and Kainan Wang. "A novel time synchronization method for smart grid based on improved wolf colony algorithm-cuckoo search optimized fuzzy PID controller." *IEEE Access* 10 (2022): 116959-116971.

[11] Benfatma, Hadjer, Houari Khouidmi, and Boubaker Bessedik. "Neural network and ACO algorithm-tuned PI controller for MPPT in a hybrid battery-supercapacitor energy storage system within DC micro-grid photovoltaic installations." *Journal of Energy Storage* 120 (2025): 116499.

[12] Fan, Hui, Hongbo Wu, Shilin Li, Shengfeng Han, Jingtao Ren, Shuo Huang, and Hongbo Zou. "Optimal Scheduling Method of Combined Wind–Photovoltaic–Pumped Storage System Based on Improved Bat Algorithm." *Processes* 13, no. 1 (2025): 101.

[13] Talebi, Shiva, and Hamed H. Aly. "Optimized Renewable Energy Integration: Advanced Modeling, Control and Design of a Standalone Microgrid Using Hybrid FA-PSO." *IEEE Access* (2025).

[14] Tang, H. H., & Ahmad, N. S. (2024). Fuzzy logic approach for controlling uncertain and nonlinear systems: a comprehensive review of applications and advances. *Systems Science & Control Engineering*, *12*(1), 2394429.

[15] Li, Jiahao, Shuai Lu, and Jing Yang. "Multi-Stage Cooperative Optimization Control for Photovoltaic MPPT: A High-Efficiency Gray Wolf Optimizer–Incremental Conductance Hybrid Strategy." *Energies* 18, no. 8 (2025): 1977.

[16] Jegajothi, B., Sundaram Arumugam, Neeraj Kumar Shukla, I. Kathir, P. Yamunaa, and Monia Digra. "An Efficient MPPT Tracking in Solar PV System with Smart Grid Enhancement Using CMCMAC Protocol." *Computer Systems Science & Engineering* 47, no. 2 (2023).

[17] Long, Wen, Ming Xu, Jianjun Jiao, Tiebin Wu, Mingzhu Tang, and Shaohong Cai. "A velocity-based butterfly optimization algorithm for high-dimensional optimization and feature selection." *Expert Systems with Applications* 201 (2022): 117217.

[18] El-Shorbagy, Mohammed A., Anas Bouaouda, Laith Abualigah, and Fatma A. Hashim. "Atom Search Optimization: a comprehensive review of its variants, applications, and future directions." *PeerJ Computer Science* 11 (2025): e2722.

[19] García-López, Adrian, Oscar Chávez-Bosquez, José Hernández-Torruco, and Betania Hernández-Ocaña. "JMetaBFOP: A tool for solving global optimization problems." *SoftwareX* 23 (2023): 101452.

[20] Li, Jie, Li Song, and Lianglin Cao. "An improved firefly algorithm with distance-guided selection strategy and its application." *Journal of Intelligent & Fuzzy Systems* 43, no. 1 (2022): 889-906.

[21] Resende, Ênio Costa, Marcelo Godoy Simões, and Luiz Carlos Gomes Freitas. "Anti-islanding techniques for integration of inverter-based distributed energy resources to the electric power system." *IEEE Access* 12 (2024): 17195-17230.

[22] Che, Yanhui, and Dengxu He. "An enhanced seagull optimization algorithm for solving engineering optimization problems." *Applied Intelligence* 52, no. 11 (2022): 13043-13081.

[23] Alsubai, Shtwai, Harish Garg, and Abdullah Alqahtani. "A novel hybrid MSA-CSA algorithm for cloud computing task scheduling problems." *Symmetry* 15, no. 10 (2023): 1931.

[24] Ma, Qianli. "Teaching Optimization Algorithm and Simulation Analysis based on Self-learning Mechanism and Multi-class Interaction." *Scalable Computing: Practice and Experience* 25, no. 4 (2024): 2398-2410.

[25] Krishnaraj, Sathyaseelan, and S. Sarathambekai. "Enhanced SVM Optimization for Diabetes Prediction Using Particle Swarm and Differential Evolution Techniques." In *Synergizing Data Envelopment Analysis and Machine Learning for Performance Optimization in Healthcare*, pp. 373-398. IGI Global Scientific Publishing, 2025.

[26] Al-Tameemi, Z. H. A., Lie, T. T., Foo, G., & Blaabjerg, F. (2022). Optimal coordinated control of DC microgrid based on hybrid PSO–GWO algorithm. *Electricity*, *3*(3), 346-364.

[27] Li, Y., Yu, H., Jiang, C., & Jin, Y. (2025). WOA–PSO of fractional-order PID control for arc plasma power supply inverter modules. *Journal of Power Electronics*, *25*(2), 382-392.

[28] Kumar, S., Gupta, A., & Bindal, R. K. (2024). Load-frequency and voltage control for power quality enhancement in a SPV/Wind utility-tied system using GA & PSO optimization. *Results in Control and Optimization*, *16*, 100442.

[29] Samal, P., Ganguly, S., & Mohanty, S. (2019). A fuzzy pragmatic DE–CSA hybrid approach for unbalanced radial distribution system planning with distributed generation. *Soft Computing*, *23*(23), 12317-12330.

[30] Sahu, P. C., Prusty, R. C., & Panda, S. (2020). Approaching hybridized GWO-SCA based type-II fuzzy controller in AGC of diverse energy source multi area power system. *Journal of King Saud University-Engineering Sciences*, *32*(3), 186-197.

[31] Maroua, B., Laid, Z., Benbouhenni, H., Elbarbary, Z. M. S., Colak, I., & Alammar, M. M. (2025). Genetic algorithm type 2 fuzzy logic controller of microgrid system with a fractional-order technique. *Scientific reports*, *15*(1), 6318.

[32] Abad-Alcaraz, V., Castilla, M., & Álvarez, J. D. (2024). A Comparison of Classical and Reinforcement Learning-based Tuning Techniques for PI controllers. *IFAC-PapersOnLine*, *58*(7), 180-185.

[33] Bahabri, M. O., Ramdas, S. K., & Banawi, H. A. (2025). Artificial neural network based hierarchical intelligent control framework for a residential microgrid. *Scientific Reports*.

[34] González-Rivera, E., García-Triviño, P., Sarrias-Mena, R., Torreglosa, J. P., Jurado, F., & Fernández-Ramírez, L. M. (2021). Model predictive control-based optimized operation of a hybrid charging station for electric vehicles. *IEEE Access*, *9*, 115766-115776.

[35] Song, Q., Yu, L., Li, S., Hanajima, N., Zhang, X., & Pu, R. (2023). Energy Dispatching Based on an Improved PSO-ACO Algorithm. *International Journal of Intelligent Systems*, *2023*(1), 3160184.

[36] Makhlouf, A., Benmachiche, A., & Boutabia, I. (2024). Enhanced Autonomous Mobile Robot Navigation Using a Hybrid BFO/PSO Algorithm for Dynamic Obstacle Avoidance. *Informatica*, *48*(17).

[37] Kala, P., Jately, V., Sharma, A., Joshi, J., Kotb, H., AboRas, K. M., & Elrashidi, A. (2024). GWO-NR hybrid method for selective harmonic elimination in multilevel inverter for distributed energy systems. *IEEE Access*, *12*, 27957-27972.

[38] Dib, F., & Boumhidi, I. (2017). Hybrid algorithm DE–TLBO for optimal H∞ and PID control for multi-machine power system. *International Journal of System Assurance Engineering and Management*, *8*(Suppl 2), 925-936.

[39] Rajamani, M. P. E., Murugappan, M., Prakash, N. B., Nair, G., & Trabelsi, M. (2024). Photovoltaic-based dual output DC–DC converter using gravitational search algorithm-tuned PI and sliding mode controllers. *Arabian Journal for Science and Engineering*, *49*(12), 16299-16317.

[40] Li, R., Gao, L., Yu, N., Li, J., Liu, Y., Wang, E., & Feng, X. (2021). Memetic strategy of particle swarm optimization for one-dimensional magnetotelluric inversions. *Mathematics*, *9*(5), 519.

[41] Yue, X., Zhang, J., Guo, J., Li, J., & Chen, D. (2024). The optimization and operation of multi-energy-coupled microgrids by the improved fireworks algorithm-shuffled frog-leaping algorithm. *PeerJ Computer Science*, *10*, e2139.

[42] Shareef, S. M., & Rao, R. S. (2022). Adaptive Grey Wolf based on Firefly algorithm technique for optimal reactive power dispatch in unbalanced load conditions. *Journal of Current Science and Technology*, *12*(1), 11-31.

[43] Xu, X., Rong, H., Trovati, M., Liptrott, M., & Bessis, N. (2018). CS-PSO: chaotic particle swarm optimization algorithm for solving combinatorial optimization problems. *Soft Computing*, *22*(3), 783-795.

[44] Chrouta, J., Farhani, F., & Zaafouri, A. (2021). A modified multi swarm particle swarm optimization algorithm using an adaptive factor

selection strategy. *Transactions of the Institute of Measurement and Control*, 01423312211029509.

[45] Alam, S. J., Arya, S. R., & Jana, R. K. (2021). Biogeography based optimization strategy for UPQC PI tuning on full order adaptive observer based control. *IET Generation, Transmission & Distribution*, *15*(2), 279-293.

[46] Al-Tameemi, Z. H. A., Lie, T. T., Foo, G., & Blaabjerg, F. (2022). Optimal coordinated control of DC microgrid based on hybrid PSO–GWO algorithm. *Electricity*, *3*(3), 346-364.

[47] Nguyen-Van, S., Lieu, Q. X., Xuan-Mung, N., & Nguyen, T. T. N. (2022). A new study on optimization of four-bar mechanisms based on a hybrid-combined differential evolution and Jaya algorithm. *Symmetry*, *14*(2), 381.

[48] Nayak, S., Kar, S. K., Dash, S. S., Vishnuram, P., Thanikanti, S. B., & Nastasi, B. (2022). Enhanced salp swarm algorithm for multimodal optimization and fuzzy based grid frequency controller design. *Energies*, *15*(9), 3210.

[49] Abdulwahab, I., Olaniyan, A. A., Musa, U., & Ajayi, O. O. (2021). Optimization of a droop controlled micro-grid using grasshopper optimization algorithm. *Zaria J.*, *10*(1), 65.

[50] Mugemanyi, S., Qu, Z., Rugema, F. X., Dong, Y., Wang, L., Bananeza, C., ... & Mutabazi, E. (2023). Marine predators algorithm: A comprehensive review. *Machine Learning with Applications*, *12*, 100471.

[51] Zishan, F., Akbari, E., Montoya, O. D., Giral-Ramírez, D. A., & Molina-Cabrera, A. (2022). Efficient PID control design for frequency regulation in an independent microgrid based on the hybrid PSO-GSA algorithm. *Electronics*, *11*(23), 3886.

[52] Deng, W., Shang, S., Cai, X., Zhao, H., Song, Y., & Xu, J. (2021). An improved differential evolution algorithm and its application in optimization problem. *Soft Computing-A Fusion of Foundations, Methodologies & Applications*, *25*(7).

[53] Fajuke, I. (2023). Optimal tuning of PID controller for speed control of DC motor using equilibrium optimizer. *The Indonesian Journal of Electrical Engineering and Computer Science (IJEECS)*.

[54] Amin, M. N., Soliman, M. A., Hasanien, H. M., & Abdelaziz, A. Y. (2021). Hybrid CSA-GWO algorithm-based optimal control strategy for efficient operation of variable-speed wind generators. In *Control and operation of grid-connected wind energy systems* (pp. 227-245). Cham: Springer International Publishing.

[55] Yusubov, E., & Bekirova, L. (2022, October). Adaptive Metaheuristic Moth-Flame Optimized Droop Control Method for DC Microgrids. In *2022 International Conference Automatics and Informatics (ICAI)* (pp. 204-209). IEEE.

[56] Memon, A. S., Laghari, J. A., Bhayo, M. A., Khokhar, S., Chandio, S., & Memon, M. S. (2023). Tunicate Swarm Algorithm based Optimized PID controller for automatic generation control of two area hybrid power system. *Journal of Intelligent & Fuzzy Systems*, *45*(2), 2565-2578.

[57] Dhriyyef, M., El Mehdi, A., & Benzaouia, M. (2025). Hybrid SSA-FA Algorithm for Efficient Appliance Scheduling in Home Energy Management Systems. *International Journal on Technical and Physical Problems of Engineering (IJTPE)*, *17*(1), 237-246.

[58] Qais, M. H., Hasanien, H. M., Alghuwainem, S., & Loo, K. H. (2023). Propagation search algorithm: a physics-based optimizer for engineering applications. *Mathematics*, *11*(20), 4224.

[59] Nallolla, C. A., P, V., Chittathuru, D., & Padmanaban, S. (2023). Multi-objective optimization algorithms for a hybrid AC/DC microgrid using RES: A comprehensive review. *Electronics*, *12*(4), 1062.

[60] Qiu, W., Guo, H., Ma, Z., & Gong, Y. J. (2025, July). A Novel Two-Phase Cooperative Co-evolution Framework for Large-Scale Global Optimization with Complex Overlapping. In *Proceedings of the Genetic and Evolutionary Computation Conference Companion* (pp. 507-510).

[61] Kesavan, P. K., Subramaniam, U., Almakhles, D. J., & Selvam, S. (2024). Modelling and coordinated control of grid connected photovoltaic, wind turbine driven PMSG, and energy storage device for a hybrid DC/AC microgrid. *Protection and Control of Modern Power Systems*, *9*(1), 154-167.

[62] Park, J., Yu, C., Min, S., Shim, J. I., & Shin, D. S. (2023). Extracting the inherent ideality factor of a diode from electrical current–voltage characteristics. *Electronics Letters*, *59*(23), e13046.

[63] Fathy, A., Alharbi, A. G., Alshammari, S., & Hasanien, H. M. (2022). Archimedes optimization algorithm based maximum power point tracker for wind energy generation system. *Ain Shams Engineering Journal*, *13*(2), 101548.

[64] Prakash, S., Arunraj, A., Paranthaman, A., & Kishore, R. (2025, August). Wind Based DFIG Integrated Grid System Using Adaptive P&O Based MPPT Controller. In *2025 8th International Conference on Circuit, Power & Computing Technologies (ICCPCT)* (pp. 352-357). IEEE.

[65] Aeggegn, D. B., Nyakoe, G. N., & Wekesa, C. (2024). ANFIS-Controlled Boost and Bidirectional Buck-Boost DC-DC Converters for Solar PV, Fuel Cell, and BESS-Based Microgrid Application. *International Transactions on Electrical Energy Systems*, *2024*(1), 6484369.

[66] Lundberg, M., Samuelsson, O., & Hillberg, E. (2022). Local voltage control in distribution networks using PI control of active and reactive power. *Electric Power Systems Research*, *212*, 108475.

[67] Martins, O. O., Oosthuizen, C. C., & Desai, D. A. (2025). Comparative analysis of evolutionary algorithms for optimising proportional–integral–derivative control in direct current motor speed regulation: A statistical evaluation. *Journal of Algorithms & Computational Technology*, *19*, 17483026251376985.

[68] Liu, Y., Zhang, H., Zheng, H., Li, Q., & Tian, Q. (2025). A spherical vector-based adaptive evolutionary particle swarm optimization for UAV path planning under threat conditions. *Scientific Reports*, *15*(1), 2116.

[69] Ahmad, M. F., Isa, N. A. M., Lim, W. H., & Ang, K. M. (2022). Differential evolution: A recent review based on state-of-the-art works. *Alexandria Engineering Journal*, *61*(5), 3831-3872.

[70] Shehab, M., & Abualigah, L. (2022). Opposition-based learning multi-verse optimizer with disruption operator for optimization problems. *Soft Computing*, *26*(21), 11669-11693.